ARTICLE

COPII collar defines the boundary between ER and ER exit site and does not coat cargo containers

Olga Shomron[1], Inbar Nevo-Yassaf[1], Tamar Aviad[1], Yakey Yaffe[1], Eitan Erez Zahavi[2], Anna Dukhovny[3], Eran Perlson[2], Ilya Brodsky[4], Adva Yeheskel[5], Metsada Pasmanik-Chor[5], Anna Mironov[6], Galina V. Beznoussenko[6], Alexander A. Mironov[6], Ella H. Sklan[3], George H. Patterson[7], Yoji Yonemura[8], Mara Sannai[8], Christoph Kaether[8], and Koret Hirschberg[1]

COPII and COPI mediate the formation of membrane vesicles translocating in opposite directions within the secretory pathway. Live-cell and electron microscopy revealed a novel mode of function for COPII during cargo export from the ER. COPII is recruited to membranes defining the boundary between the ER and ER exit sites, facilitating selective cargo concentration. Using direct observation of living cells, we monitored cargo selection processes, accumulation, and fission of COPII-free ERES membranes. CRISPR/Cas12a tagging, the RUSH system, and pharmaceutical and genetic perturbations of ER-Golgi transport demonstrated that the COPII coat remains bound to the ER–ERES boundary during protein export. Manipulation of the cargo-binding domain in COPII Sec24B prohibits cargo accumulation in ERES. These findings suggest a role for COPII in selecting and concentrating exported cargo rather than coating Golgi-bound carriers. These findings transform our understanding of coat proteins' role in ER-to-Golgi transport.

Introduction

The first sorting stations for proteins in the secretory pathway are ER exit sites (ERESs; Balch et al., 1994). These are specialized membrane domains on the surface of the ER that are identified by the COPII heterocomplex and ER-Golgi recycling proteins such as ERGIC53 (Schindler et al., 1993). The COPII protein complex has been identified in yeast and mammalian cells as a membrane coat involved in anterograde trafficking from the ER (Barlowe et al., 1994; Kirk and Ward, 2007). The complex formation is initiated by the Sar1 small GTPase, which is recruited to the ER membrane by Sec12, a protein that acts as its GDP-to-GTP exchange factor. Sar1 recruitment triggers the assembly of Sec23/24 subcomplexes with cargo proteins, and then Sec13/31 forms the outer cage of the coat (Aridor, 2018; Peotter et al., 2019; Zanetti et al., 2011). The assembling lattice deforms the membrane to become spherical or tubular membrane structures (Mancias and Goldberg, 2008; Zanetti et al., 2013). Mezzacasa and Helenius (2002) demonstrated that the COPII-labeled transitional ER defines the quality control boundary, after

which misfolded proteins are not retrieved back to the ER. COPII machinery is involved in cargo recruitment, sorting, and exit out of the ER (Aridor, 2018; Barlowe and Helenius, 2016; Gomez-Navarro and Miller, 2016; Zanetti et al., 2011). However, in mammalian cells, the existence of COPII vesicles is still controversial (Mironov and Beznoussenko, 2019; Mironov et al., 2003; Zeuschner et al., 2006). Recent research focused on large cargo proteins such as procollagen stimulated alternative or additional hypotheses about the role of COPII components in cargo sorting, concentration, and export from the ER (Saito et al., 2009). Large procollagen-containing COPII carriers were described (Gorur et al., 2017; Yuan et al., 2018), but more and more data show that, alternatively, large cargo leaves the ER without COPII (McCaughey et al., 2019). TANGO, an ER resident protein, together with cTAGE5, is associated with mediating the interaction between soluble cargo proteins and COPII to facilitate their export from the ER (Saito et al., 2009; Saito et al., 2011). COPII with TANGO's help may function by forming a collar that

restricts and controls access to post-ER compartments (Raote et al., 2017; Raote et al., 2018; Santos et al., 2015). Following these findings, COPII was shown to be required for stringent ER retention of misfolded and ER resident proteins (Ma et al., 2017).

Here, living intact cells expressing fluorescent protein (FP)–tagged COPII either transiently or via knock-in at endogenous levels were used to visualize ER-to-Golgi trafficking of FP-tagged cargo. We found that carrier fission, the earlier step of cargo selection, and FP-tagged cargo accumulation occur essentially downstream from COPII-labeled membranes. Confocal and immunoelectron microscopy of cells treated with Brefeldin A (BFA) and nocodazole (Noc) demonstrated that COPII defines the ER–ERES boundary, facilitating cargo selection and concentration in ERES membranes. Using mutagenesis to perturb cargo binding of COPII, we found that cargo accumulated in the ER, thus supporting COPII localization and function at the ER–ERES boundary. Furthermore, we demonstrate that a subpopulation of COPI is localized to ERESs and is also seen on ER-to-Golgi anterograde carriers. Our data suggest a revised model for COPII functioning as a stable gatekeeper at the ERES boundary rather than as a transient coat of transport carriers.

Results

The distribution of ER exit sites

The well-established ERES distribution (Stephens et al., 2000) was confirmed using our markers expressed in living intact cells. To determine the robustness of our findings, we used COS7, HeLa, and Huh7 cell lines. The COPII subunit mCherry-Sec24C was coexpressed either with the FP-tagged ER marker reticulon or VSVG (Fig. 1 A). Fig. 1 B and Video 1 demonstrate the distribution of ERESs in living HeLa cells coexpressing COPII Sec13-mCherry and the secretory transport of VSVG-EGFP at permissive temperature of 32°C. In these cells, we also demonstrate that VSVG secretory traffic is indistinguishable from what is reported in other cell lines (Hirschberg et al., 1998). Upon temperature shift, the ER-resident VSVG is transported to the Golgi apparatus and further to the cell surface. The Sec13-mCherry is under endogenous expression as the mCherry tag was knocked in at the Sec13 C terminus using CRISPR/Cas12a (Fueller et al., 2020). The characterization of this cell line is detailed in Fig. S1. In these cells, Sec13-mCherry shows the typical intracellular distribution of ERESs and, in so doing, also serves as a control for experiments where fluorescently labeled COPII subunits (Sec13, Sec24B, Sec24C, and Sec23) were transiently expressed. In either type of experimental system, the intracellular distributions of COPII subunits appeared identical.

COPII membranes are stable and immobile

Next, we compared the lateral movement of membrane-associated COPII with ER-to-Golgi cargo carriers and plus-ends growth of microtubules labeled with GFP-EB3 in living intact cells. Fig. 2 A shows a maximum-intensity projection of 50 consecutive frames taken at 0.66-s intervals (see also Video 2). Compared with the rapid movement of transport carriers covering significant distances along microtubular tracks toward the Golgi apparatus, COPII-labeled membranes are practically

immobile. Similar results are obtained when COPII-labeled membranes are compared with microtubule plus-end tip progression using GFP-EB3 (Fig. 2 B and Video 3). Thus, at the time frame of 3 min when carriers or microtubule plus-ends cover a distance of 10s of microns, COPII membranes are nearly stable and immobile with only minor local random movements.

Additionally, using EB3, the secretory pathway is at a steady-state compared with cells expressing VSVG, where a large mass of cargo is released from the ER. In both states, COPII-labeled membranes are stationary. These data are consistent with early observations (Hammond and Glick, 2000; Stephens et al., 2000; Westrate et al., 2020) and support the idea that COPII membranes are involved in recruiting but not transporting cargo.

Cargo accumulation and fission occur downstream from stationary COPII-coated membranes

As membrane-bound COPII is stable and stationary, we analyzed the early stages of ER export of VSVG. ER export was visualized at the level of a single ERES in a living intact cell. To this end, cells coexpressing the cargo protein VSVG-YFP and the COPII subunit Sec24C-mCherry were shifted to permissive temperature (32°C) after overnight incubation at the nonpermissive temperature of 39.5°C. Fig. 3 A and Video 4 show the dynamics of ER export in a single ERES in a living cell. Cargo is primarily concentrated and accumulated in growing dynamic tubular membranes that mostly do not overlap with COPII membranes and later bud as a whole.

Moreover, during multiple cycles of cargo accumulation and fission, COPII membranes are stable and stationary. Cargo accumulation and carrier fission are coupled and continuous processes. They can only be distinguished at a higher spatio-temporal resolution, as in Fig. 3 B, Video 5, Video 6, Video 7, and Video 8. Based on these image sequences, the first stage is cargo accumulation in ERES membranes (Fig. 3 B, two top panels). Subsequently, these membranes undergo fission to become membrane carriers (Fig. 3 B, two bottom panels). A key observation is that fission sites occur on contiguous ERES membranes adjacent yet segregated from COPII-coated membranes. COPII does not localize to these growing tubular membranes where the cargo is accumulating but instead remains at the tubule base without changing its intensity. An identical cargo accumulation pattern as proliferating dynamic round-shaped or tubular elements and carrier fission is apparent for other types of cargo such as the RUSH-TNF (Boncompain et al., 2012; Fig. 3 C). Also, using the knock-in Sec13-mCherry HeLa cell line transfected with VSVG-GFP (Fig. 3, D and E) and using RUSH-TNF (data not shown) show identical results.

The life history of ER-to-Golgi carriers: Rab1 colocalizes with cargo to the Golgi apparatus

Next, we sought to follow the transport carriers that bud from ERESs to the Golgi apparatus. The knock-in Sec13-mCherry HeLa cells were transfected with VSVG-GFP. About 10 min after the shift to permissive temperature (32°C), the VSVG-GFP within the region of interest surrounding the Golgi was photobleached with a high-power laser (Fig. 4 A) before capturing the image sequence. Fig. 4 B shows selected images and a projection
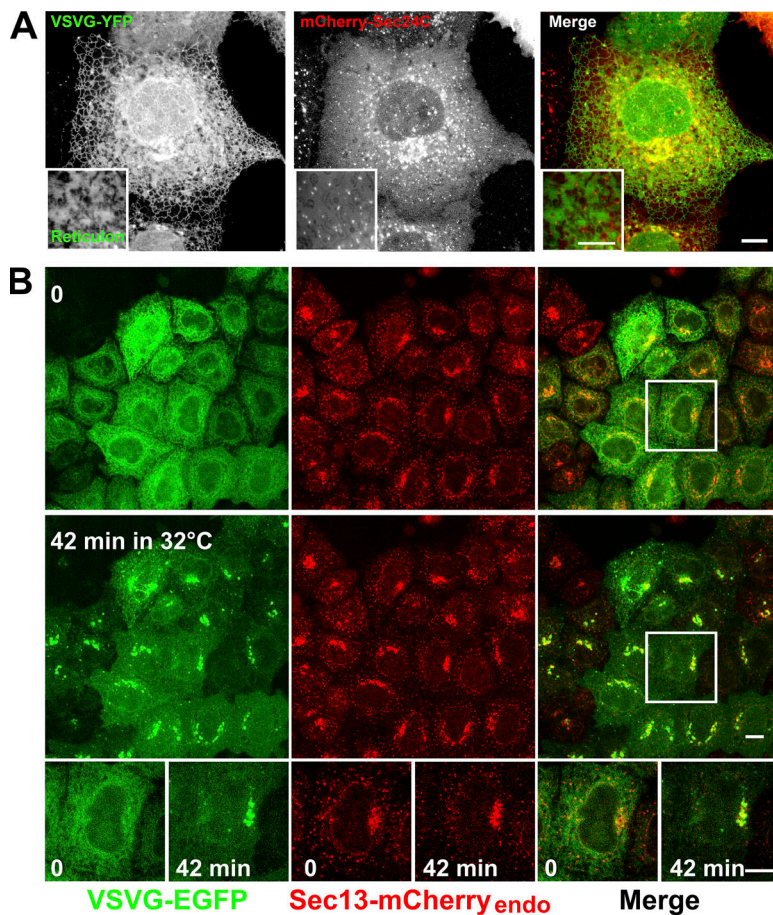
Figure 1. **Intracellular distribution of ERESs using FP-tagged COPII expressed in living intact cells. (A)** Intracellular distribution of ERESs. A confocal image of a COS7 cell co-expressing the ER marker VSVG-YFP (left and green in merged image) at the nonpermissive temperature 39.5°C or the ER membrane marker reticulon-GFP (left insert and green in merged insert) and the COPII subunit Sec24C-mCherry (center, and red in merged image). Scale bars = 5 μm. **(B)** A HeLa cell clone expressing an endogenous (endo) Sec13-mCherry (red) inserted using the CRISPR/CAS12 knock-in method were transfected with VSVG-EGFP (green). Cells were transferred to permissive temperature (32°C) after an overnight incubation at 39.5°C, and images were taken at 15-s intervals for ~40 min. See Video 1. Shown are images at 0 and 40 min. Scale bars = 5 μm.

demonstrating a transport carrier budding from an ERES and translocating to connect to the Golgi apparatus (see also Video 9). Next, we attempted to follow the life history of ER-to-Golgi carriers using the Rab1 molecular switch. Rab1, part of the early secretory transport machinery, was recently reported on ERESs and transport vesicles (Westrate et al., 2020). Fig. 4 C shows selected images of Huh7 cells cotransfected with VSVG-GFP and Rab1b-mCherry and incubated overnight at the nonpermissive temperature of 39.5°C. Cells were transferred to permissive temperature, and confocal images were captured at 0.8-s intervals. The path from the ERES to the Golgi apparatus of the transport carriers is also shown in the projection and Video 10. Both Rab1 and VSVG colocalization are observed on ERES and transport carriers throughout their path to the Golgi. These data demonstrate that VSVG containing ERES membranes apparently bud and move directly to the Golgi apparatus. Unlike COPII, Rab1b is bound to the carrier membrane throughout its lifetime. Furthermore, our ability to visualize the carrier membrane–bound subpopulation of the small GTPase Rab1, on the background of its soluble form, argues against the view that carrier-bound COPII is below detection levels.

COPII localizes to the ER–ERES boundary, where it mediates selective cargo sorting, and concentration in Noc-BFA–treated cells

Next, we asked to establish the relative localization of ERES, COPII-coated, and ER membranes. To this end, we used a previously reported experimental system where cells are simultaneously treated with BFA and Noc (Dukhovny et al., 2008). We found that the simultaneous inhibition of both Arf1 activation by BFA (Lippincott-Schwartz et al., 1989) and microtubules polymerization by Noc (Hirschberg et al., 1998) preserves the COPII-mediated cargo sorting functions within ERESs while blocking the subsequent exit of cargo from the ER (Dukhovny et al., 2008). Release of VSVG-YFP at permissive temperature in the presence of BFA and Noc results in active COPII-mediated sorting of VSVG-YFP into ERES membranes that now transform at the light microscope level into growing spherical structures (Fig. 5 A, Fig. S2, Video 11, and Video 12; Dukhovny et al., 2008; Yonemura et al., 2016). Another key feature of BFA/Noc treatment is that the COPII-cargo segregation is effectively visually emphasized. ERES membrane growth is a direct outcome of COPII-mediated cargo selection, sorting, and accumulation (Fig. S2). The localization of endogenous COPII was verified using immunofluorescence with antibodies against Sec24C (Fig. S2). The effect shown in Fig. 5 A is not a side effect of BFA and Noc because it could be reproduced using Golgicide A and colchicine, a BFA analogue with the same target, and a microtubule polymerization inhibitor (Sáenz et al., 2009), respectively (Fig. S2). A variety of cargo proteins could be localized to the ERES membrane under BFA and Noc: WT CFTR, GalT, and ERGIC53 (Fig. 5 B and Fig. S2). Interestingly, ERGIC53 under BFA/Noc treatment is restricted to the ER and is concentrated in ERES membranes indistinguishable from any other type of exported
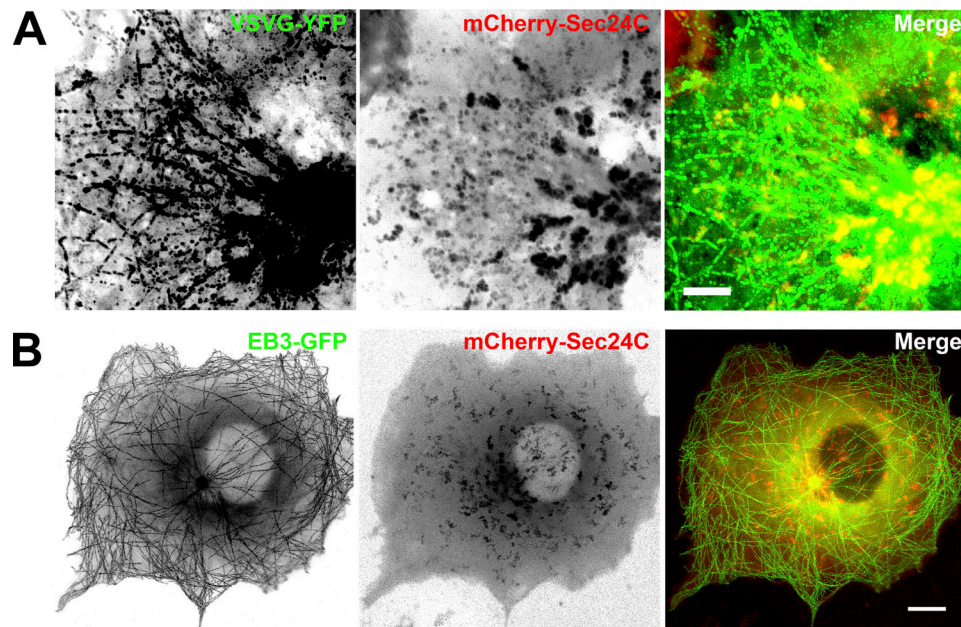
Figure 2. **Membrane-associated COPII is stationary compared with cargo vesicle movement and microtubule plus-end polymerization. (A)** Comparison between membrane-associated COPII movement and transport of ER-to-Golgi carriers. An inverted brightest pixel projection of 50 images from a 0.66-s interval time-lapse sequence of COS7 cell coexpressing VSVG-YFP (left, and green in merged image) and the COPII subunit Sec24C-mCherry (center, and red in merged image) after a shift to permissive temperature (32°C). See Video 2. Scale bar = 5 μm. **(B)** Comparison between membrane-associated COPII and microtubule plus-end polymerization using EB3-GFP. An inverted brightest pixel projection of 50 images from a 3.7-s interval time-lapse sequence of COS7 coexpressing EB3-GFP (left, and green in merged image) and the COPII subunit Sec24C-mCherry (center, and red in merged image). See Video 3. Scale bar = 10 μm.

cargo. Next, localization of the membrane-bound COPII collar relative to both cargo-enriched membranes and the ER was determined using deconvolved confocal microscopy analysis of living BFA/Noc-treated cells (Fig. 5 C, Video 11, and Video 12). These data demonstrate that membrane-bound COPII is consistently positioned between the ER and ERESs. To verify whether the membrane and lumen of ERESs in BFA/Noc-treated cells are at all times continuous with those of the ER, we coexpressed mCherry with a cleavable signal sequence with VSVG-YFP. The signal sequence confers insertion into the ER lumen and its further secretion. The continuous lumen labeled with mCherry shown in Fig. 5 D and Video 13 confirms that ERESs under BFA/Noc are linked to the ER. To demonstrate that COPII can distinguish between transport-competent and -incompetent proteins in BFA/Noc-treated cells, we compared COPII-mediated sorting of WT and the Δ508 transport-incompetent mutant of CFTR. While WT CFTR accumulates in ERESs, the transport-incompetent misfolded mutant protein CFTR-Δ508 is excluded from ERESs (Fig. S2; Wang et al., 2004). These data demonstrate that COPII is functional in BFA/Noc: the membrane-bound COPII collar identifies and excludes transport-incompetent misfolded mutant proteins from entering ERESs. Moreover, cargo accumulation proceeds at a normal rate compared with untreated cells (Fig. S2; Dukhovny et al., 2008). ERESs in BFA/Noc-treated cells coexpressing the COPII subunit Sec24C and cargo were monitored using high-speed confocal microscopy to follow cycles of membrane (Fig. S2 and Video 14) and cargo accumulation. The membrane-bound COPII fluorescence levels were indifferent to the undulating cargo concentrations within ERES

(Fig. S2 and Video 15) as seen for untreated cells (Fig. 3). This result is consistent with COPII stably occupying the ER–ERES boundary. At the light microscopy level, COPII forms a collar that localizes between ER and ERES membranes. To study the ultrastructure of the BFA/Noc-dilated ERESs, we performed EM using immunogold anti-GFP antibodies on cells coexpressing Sec23C-GFP and VSVG-Scarlet (Fig. 5 E). Cells used for the EM analysis were primarily examined at the light confocal level immediately after fixation (Fig. 5 E, left). The EM images of ERESs and the 3D serial sections reconstruction of the membrane structure (Fig. 5 E, bottom) reveal a highly complex topology of a hollow multilayered perforated sphere (Fig. 5 E, scheme, bottom right). These structures correspond to the membranes in which cargo is sorted and concentrated (Fig. 5 E). The scheme in Fig. 5 E, bottom right, illustrates the positioning of the section relative to the ERESs under BFA/Noc treatment. These structures were previously observed in several studies. The first set of observations reporting on analogous structures titled fenestrated spheres were from thick sectioning EM analysis of the Golgi apparatus (Rambourg and Clermont, 1992). Similar structures were also observed in BFA-treated cells and were referred to as Glumerolini (Pavelka and Ellinger, 1993). Moreover, Golgi fenestrated membranes and ERESs of BFA-treated yeast *Schizosachharomyces pombe* (Rambourg et al., 1995b) and *Saccharomyces cerevisiae* (Rambourg et al., 1995a) exhibited the same morphology and dimensional scale. The immunogold labeling of Sec23 is significantly concentrated at the base of the perforated globular membranes (Fig. 5 E, yellow arrowhead). These data underpin

Shomron et al.
COPII defines the boundary between ER and ERESs

Journal of Cell Biology   4 of 16
https://doi.org/10.1083/jcb.201907224
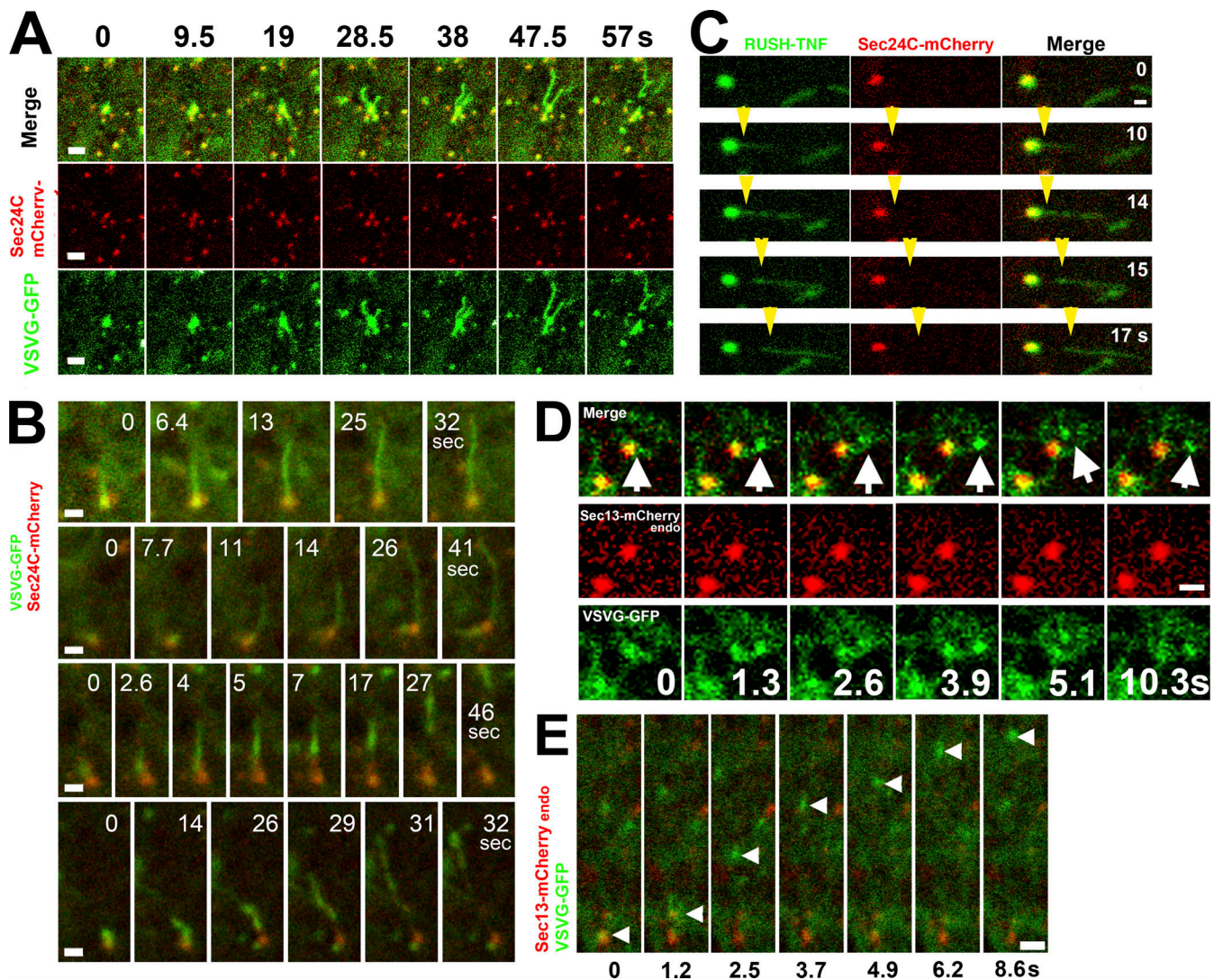
Figure 3. **Analysis of cargo accumulation and carrier formation in living cells. (A)** Accumulation of VSVG-YFP cargo and fission of carriers from ERESs in living cells. Confocal images were captured after the shift to the permissive temperature of COS7 cells coexpressing COPII subunit Sec24C-mCherry (red) and the cargo protein VSVG-YFP (green). See Video 4. Scale bar = 2 µm. **(B)** Cargo accumulation in a single ERES and carrier fission. Confocal images captured at 2.6-s intervals of COS7 cells transfected and treated as in A. VSVG-YFP (green) accumulation downstream to Sec24C-mCherry (red) is shown in two top panels and fission of carriers in the two bottom panels. See Video 5, Video 6, Video 7, and Video 8. Scale bar = 1 µm. **(C)** Analysis of ER export using the RUSH system. Images were captured after the addition of biotin to living COS7 cells 48 h after cotransfection of Sec24C-mCherry (red) and the cargo protein RUSH-TNF-GFP (green). Yellow arrowheads point to carrier elongating and budding. Scale bar = 1 µm. **(D and E)** Budding of a carrier from ERES in Sec13-mCherry (red) CRISPR/CAS12 knock-in HeLa cell clone transfected with VSVG-EGFP (green). White arrows and arrowheads point to carriers. Scale bar = 1 µm.

our observation that the membrane-bound COPII is localized between ER and ERESs.

Mutagenesis of the cargo-binding Sec24B disrupts cargo accumulation in ERESs, causing ER retention

Sec24 is a COPII subunit that directly interacts with cargo (Wendeler et al., 2007). The B isoform of Sec24 interacts with acidic export motifs found in numerous surface proteins, including VSVG and CFTR (Wang et al., 2004). To enhance the binding between Sec24B and the di-acidic motif of VSVG, we used structure-based computer modeling of Sec24B (Protein Data Bank accession no. 3EH1; Mancias and Goldberg, 2008) and designed a mutant of Sec24B by substituting valine at position 932 with the basic amino acid arginine (V932R; Fig. 6, A and B).

This substitution adds another positive charge to the already existing three arginines in the binding pocket for acidic export motifs of cargo proteins. A stronger binding of the VSVG tail by the V932R mutant than the WT was predicted by both allowed docking peptide states and surface electrostatic potential analysis (Dolinsky et al., 2007; London et al., 2011; Pettersen et al., 2004). Primarily, we confirmed that the mutant Sec24B$_{V932R}$ bound VSVG using coimmunoprecipitation (Fig. S3). Fluorescence recovery after photobleaching was measured for WT or mutant Sec24B in BFA/Noc-treated cells in the presence of coexpressed VSVG (Fig. 6 C). As predicted by the abovementioned models in Fig. 6, A and B, the results show that membrane-bound Sec24B$_{V932R}$ has a 1.5-fold slower on/off rate and a significantly smaller mobile fraction than WT Sec24B. The

Shomron et al.
COPII defines the boundary between ER and ERESs

Journal of Cell Biology 5 of 16
https://doi.org/10.1083/jcb.201907224
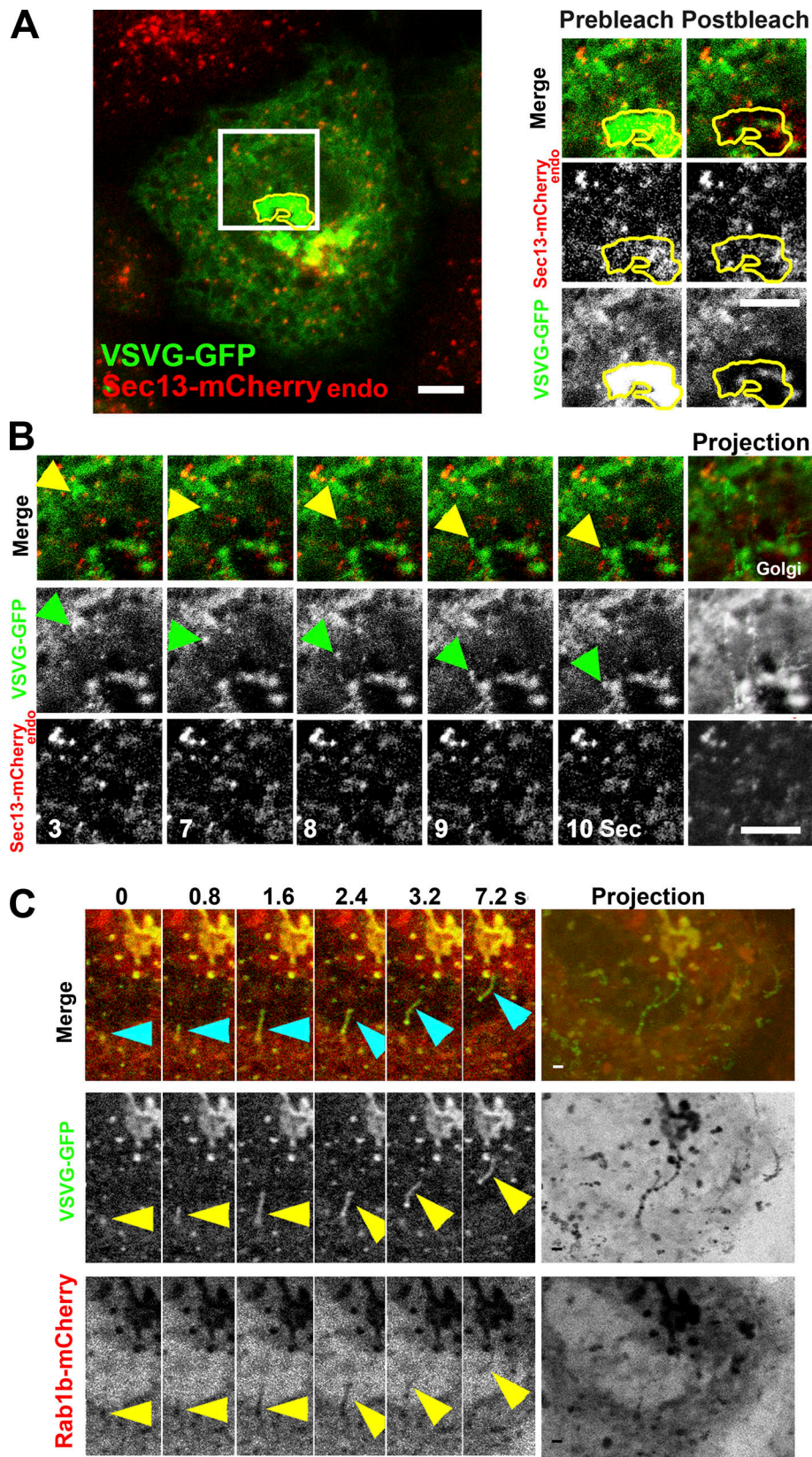
Figure 4. **Analysis of the life history of ER-to-Golgi carriers: budding translocation, fusion, and colocalization of cargo with the small GTPase Rab1b.** **(A)** Photobleaching of the Golgi to expose ER-to-Golgi carrier life history. The Golgi region of interest was photobleached in the VSVG-GFP (green) channel after transfer to permissive temperature (32°C), following overnight at 39.5°C. Cells used were a HeLa cell clone expressing an endogenous (endo) Sec13-mCherry (center, and red in merged image) transfected with VSVG-GFP (bottom, and green in merged image). Scale bars = 5 µm. **(B)** Representative images from a time-

Shomron et al.
COPII defines the boundary between ER and ERESs

Journal of Cell Biology 6 of 16
https://doi.org/10.1083/jcb.201907224

lapse series captured after the FRAP in A. Arrowheads point to carrier translocating and fusing with the Golgi. Right: Projection of the images in B. See Video 9. Scale bar = 5 µm. **(C)** Rab1b localizes with cargo throughout the life history of ER-to-Golgi carriers. Huh7 cells were cotransfected with VSVG-YFP (center, and green in merged image) and Rab1-mCherry (red and inverted, bottom), were shifted to the permissive temperature of 32°C after an overnight in nonpermissive temperature (39.5°C). Representative images captured by confocal microscopy from a time-lapse series are shown with designated times. Arrowheads point to a single carrier budding from an ERES translocating and fusing with the Golgi apparatus. Right: A projection showing the path of the same carrier. See Video 10. Scale bar = 1 µm.

on/off time scales are 4.6% × s^{-1} and 6.9% × s^{-1} for mutant and WT, respectively, are consistent with a stronger binding of cargo by Sec24B$_{V932R}$ (Fig. 6 D). Expression of Sec24B$_{V932R}$ blocked VSVG transport, causing its accumulation in the ER after release in permissive temperature (Fig. 6, E–G). Retention in the ER of cargo proteins in permissive temperature supports our previous results of the localization of membrane-bound COPII to the ER–ERES boundary, where it controls access of ER proteins to ERES. The phenotype of Sec24B$_{V932R}$ was further studied using CFTR, another di-acidic motif–containing multi-transmembrane domain surface protein (Wang et al., 2004). Fig. 6 H shows that in BFA/Noc-treated cells, CFTR-GFP is excluded from ERESs in cells coexpressing Sec24B$_{V932R}$, but not Sec24B$_{WT}$. These data demonstrate that COPII localizes and functions at the ER–ERES boundary, essentially mediating selective cargo concentration from ER via COPII-coated membranes to ERES.

Model of COPII function at the ER boundary
Implication I: Transport from ER through COPII collar to Golgi via direct membrane connection
In this study, we provide data that support an alternative hypothesis for the role of the COPII machinery in ER export. Rather than COPII-coated vesicles, we demonstrate that COPII-coated membranes form a collar that defines the boundary between the ER and ERES membranes (Fig. 7 A). The traditional mechanism described for COPII recruitment, assembly, and cargo selection is compatible with our alternative model. Specifically, ER-localized Sec12-activated Sar1 recruits the Sec24-Sec23 to the membrane at the ER side of the COPII collar. Next, the Sec23-Sec24 complex interacts with transport competent cargo, and the complex translocates to release the cargo at the ERES. The drive for this COPII-cargo complex movement toward the ERES is based on two types of well-documented interactions: non-specific interaction between cargo transmembrane domain and surrounding lipids (Fig. 7 A, top right; Dukhovny et al., 2009; Sharpe et al., 2010), and specific interaction between cargo export signal and COPII (Fig. 7 A, bottom right; Kuehn et al., 1998; Lee and Goldberg, 2010). These interactions in the context of our new model are discussed in detail in the Discussion. This model is fully compatible with the new revisited hypothesis of COPII-mediated ER–Golgi direct connectivity that is gaining momentum (Griffiths, 2000; Raote and Malhotra, 2019). A subpopulation of Golgi-associated ERESs is consistently present when labeling with COPII markers (Fig. 1, A and B; and Fig. 2, A and B). ERESs are also frequently observed adjacent to Golgi cisternae in EM studies (Fan et al., 2003; Sesso et al., 1994). After the shift to permissive temperature, we visualized VSVG-YFP accumulation in Golgi membranes that appear decorated with ERES (Fig. 7 C and Video 1). This accumulation can be interpreted at least in

part as mediated by direct transfer of cargo from ER to the Golgi via the Golgi-associated COPII domains. The simultaneous disappearance of the Golgi and subpopulation of Golgi-associated COPII domains upon BFA treatment (Video 16) provides some support for direct connectivity between ER and Golgi. Notably, under that BFA treatment, the rest of the peripheral non–Golgi-associated ERESs were apparently not affected (Ward et al., 2001).

Implication II: Evidence for COPI in anterograde traffic
The localization of COPII to the boundary between the ER and ERES membranes prompts a question about the coat protein's identity for anterograde ER-to-Golgi carriers. Several observations clearly show COPI's involvement in anterograde traffic (Scales et al., 1997; Shima et al., 1999). Both Scales et al. (1997) and Shima et al. (1999) demonstrated a sequential mode of action for COPI replacing COPII on ER-to-Golgi vesicles. COPI-positive membranes are considered as markers of the adjacent ER-Golgi intermediate compartment (Ben-Tekaya et al., 2005; Klumperman et al., 1998). However, it is still accepted in the literature that COPI is exclusively associated with retrograde transport. Confocal time-lapse microscopy of living intact LdlF cells (Presley et al., 2002) coexpressing Sec24C-mCherry and the ER marker KDEL-BFP2 demonstrated that COPI localized to Golgi apparatus membranes and Sec24C-positive ERESs (Fig. S4). Before budding, both εCOP-YFP and Sec24C-mCherry partially overlap and display local random movements as a single object on top of the ER (Video 17). Upon budding, the COPI-positive membranes rapidly move toward the Golgi. This observation challenges the retrograde role of COPI and is consistent with the idea that COPI is labeling a separate organelle such as ERGIC (Blum et al., 2000). A rapid movement toward the Golgi follows the budding of COPI membranes.

Thus, we demonstrate a new model for the function of COPII based on direct live-cell microscopy and EM. We find that COPII occupies and defines the boundary between the ER and ERESs, where it functions in cargo sorting and concentration. COPII-free cargo-loaded ERES membranes undergo fission to form ER-to-Golgi carriers.

Discussion
The COPII machinery role in the concentration of cargo has been previously reported (Farhan et al., 2007; Malkus et al., 2002) and reviewed (Gomez-Navarro and Miller, 2016). Traditionally, cargo concentration is coupled to COPII-coated vesicle formation (Béthune and Wieland, 2018). However, our data demonstrate a well-defined localization of COPII to the ER–ERES boundary. Accordingly, the membranes that accumulate cargo, transform
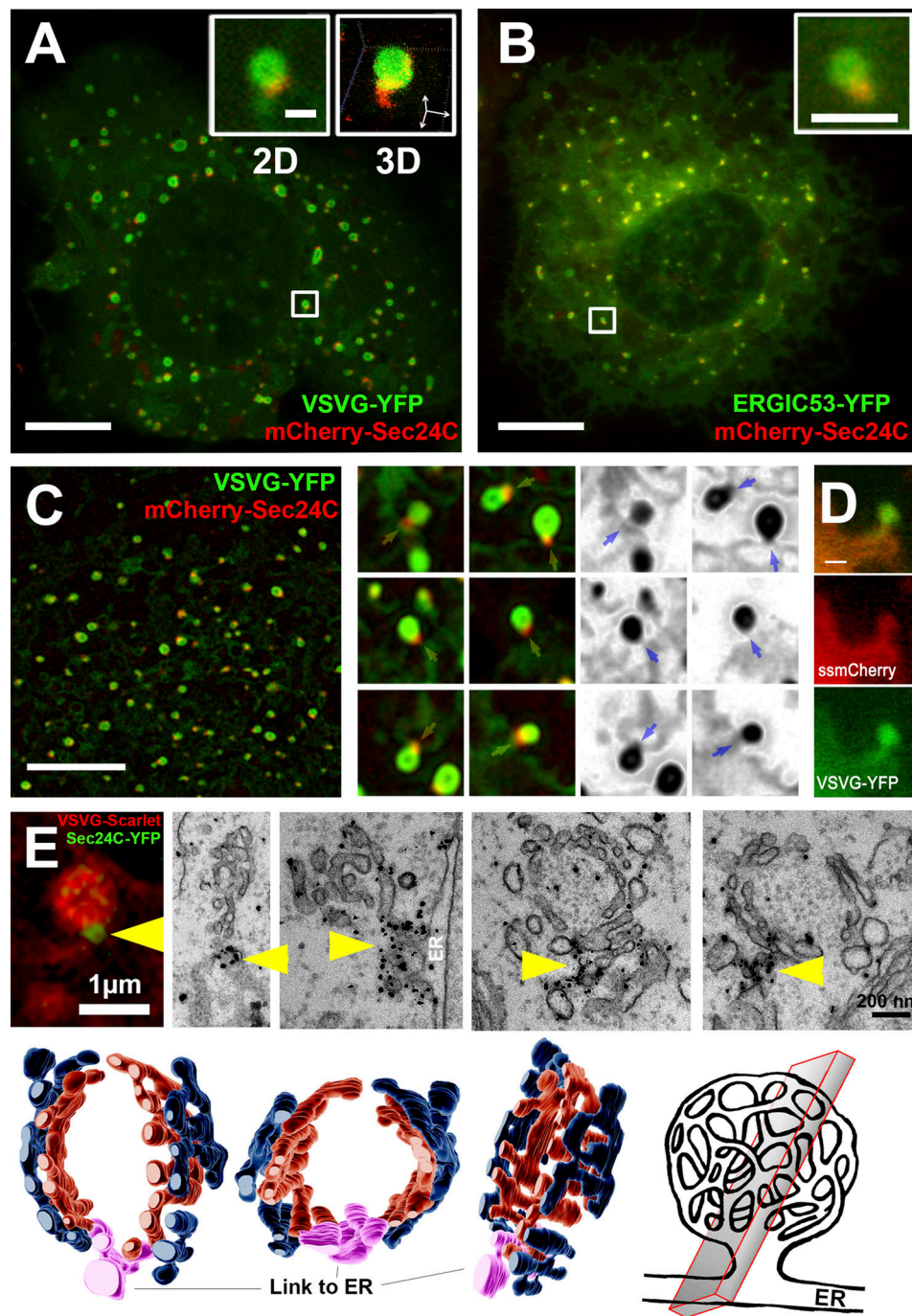
Figure 5. **Characterization and localization of COPII in ERESs in BFA/Noc-treated intact living cells. (A)** 3D confocal analysis of ERESs in BFA/Noc-treated living cells. A single confocal image from a z-section stack of a COS7 cell cotransfected with VSVG-YFP (green) and Sec24C-mCherry (red) transferred to permissive temperature (32°C) after overnight incubation at 39.5°C and treated with BFA/Noc as described in Materials and methods. The top left insert is a fivefold enlargement of a single ERES. The top right insert is a 3D reconstruction of the same ERES. Bar and white arrows are 1 μm in the x, y, and z directions. Scale bar = 10 μm. **(B)** Colocalization of ERGIC53 and COPII in ERESs under BFA/Noc treatment. COS7 cells expressing ERGIC53-YFP and the COPII subunit Sec24C-mCherry were treated with BFA/Noc as described in Materials and methods section. Inset (scale bar = 2 μm) is a fivefold enlargement of a single representative ERES. Scale bar = 10 μm. **(C)** COPII-labeled membranes separate ER and ERES membranes. Confocal deconvolved images of a COS7 cell were transfected and treated as in A. Six representative fourfold enlarged images of ERESs are shown on the right. Yellow/blue arrows point to COPII-coated collars (Sec24C-mCherry, red) intersecting between ER and ERES. The VSVG (green) channel is shown inverted on the right. See Video 11 and Video 12. Scale bar = 10 μm. **(D)** ERESs are connected to the ER in BFA/Noc-treated cells. Confocal image of a living COS7 cell cotransfected with VSVG-YFP (green) and the soluble secreted luminal marker signal sequence-mCherry (red) under BFA/Noc treatment. See Video 13. Bar = 1 μm. **(E)** Immunogold EM analysis demonstrates the transformation of ERES membranes under BFA/Noc treatment to spherical-tubular membranes known as glumerolini. Left: Confocal image of an ERES of a fixed COS7 cell expressing Sec23-GFP (green) and VSVG-Scarlet (red) under BFA/Noc treatment after 30 min at the permissive temperature 32°C. Right: Immunogold EM serial sections labeled with anti-GFP antibodies of ERESs in BFA/Noc-treated cells. Yellow arrowheads point to sites of contact to ER with increased labeling of COPII. Scale bar = 200 nm. Bottom: A 3D reconstruction of the membrane structure from serial sections. Bottom right: A scheme depicting the positioning of the section relative to the ERESs under BFA/Noc treatment.
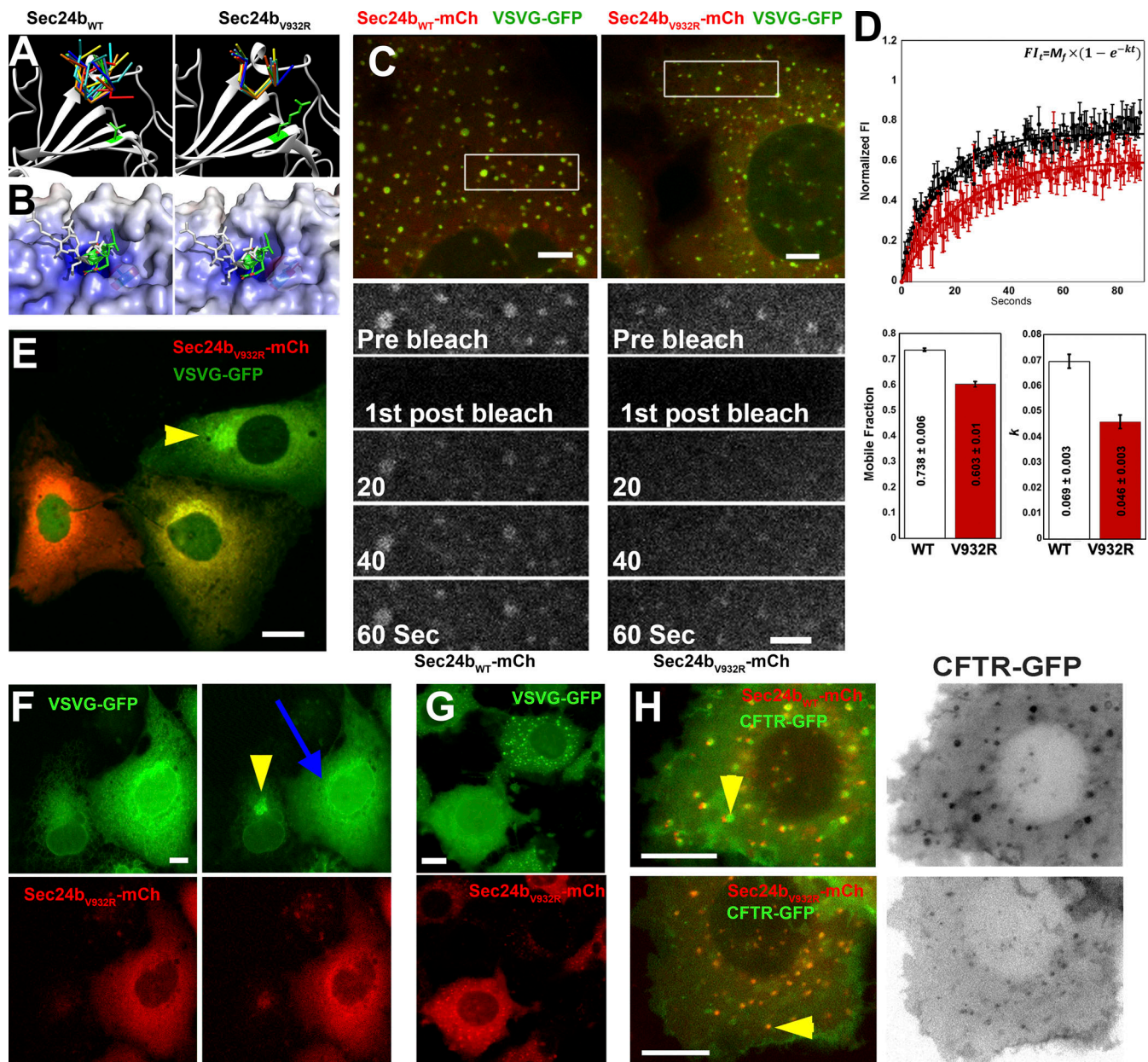
Figure 6. **A site-directed gain of function mutation of the cargo binding site of Sec24B obstructs ER export at the ER–ERES boundary. (A)** Computer modeling of the binding of Sec24B WT or the V932R mutant to the VSVG export motif. **(A)** A ribbon diagram of the crystallographic structure of the binding pocket of Sec24B is shown in gray with allowed conformations of the VSVG export motif in colors. In green are the amino acids with side chain structural representations before and after substitution. **(B)** Electrostatic potential and solvent accessibility maps demonstrate a more defined pocket for the VSVG tail binding site in the V932R mutant compared with the WT. **(C)** FRAP of COS7 cells coexpressing the VSVG-GFP (green) and the Sec24B-mCherry (red, WT on the left and V932R mutant on the right) under BFA/Noc treatment as described in Materials and methods. Images were captured after bleaching a rectangle of WT or mutant Sec24B-mCherry to follow the recovery rate. Scale bar = 5 μm. **(D)** FRAP analysis for the experiments in C. Comparison of the membrane-binding dynamics for the WT (black) or V932R mutant (red) Sec24B. To avoid background fluorescence, maximum pixel intensities within the bleach box were exclusively plotted. Data represent an average of 10–12 experiments. Data were fitted to a single exponential equation shown in the graph. Bar graphs show the average mobile fractions (left) and exponential rate constant (right) with SDs. **(E)** Dose–response of Sec24B$_{V932R}$ mutant (red) overexpression inhibiting ER-to-Golgi export of VSVG-YFP (green). Three cells with different levels of expression of Sec24B$_{V932R}$ with a corresponding degree of ER export inhibition. Arrowhead points to the Golgi apparatus. Scale bar = 10 μm. **(F)** Expression of Sec24B$_{V932R}$ causes VSVG retention in the ER. Shifting cells coexpressing the mutant Sec24B$_{V932R}$ (red) and VSVG-YFP (green) to permissive temperature results in retention of VSVG-YFP in ER (blue arrow). Yellow arrowhead points to the Golgi apparatus in a cell not expressing Sec24B$_{V932R}$. Scale bar = 10 μm. **(G)** Sec24B$_{V932R}$ prevents VSVG cargo accumulation in ERESs in BFA/Noc-treated cells. COS7 cells were cotransfected with VSVG-YFP (geen) and Sec24B$_{V923R}$-mCherry (red) and treated with Noc and BFA. Bottom left cell is expressing the Sec24B$_{V932R}$-mCherry mutant where VSVG-YFP is retained in the ER. Scale bar = 10 μm. **(H)** Sec24B$_{V932R}$ blocks the accumulation of CFTR in ERESs in BFA/Noc-treated cells. COS7 cells cotransfected with CFTR-GFP (green, inverted on the right) and either Sec24B$_{V923R}$-mCherry or Sec24B$_{WT}$-mCherry (red) were treated with Noc and BFA. Yellow arrowheads point to ERESs. Scale bars = 10 μm.
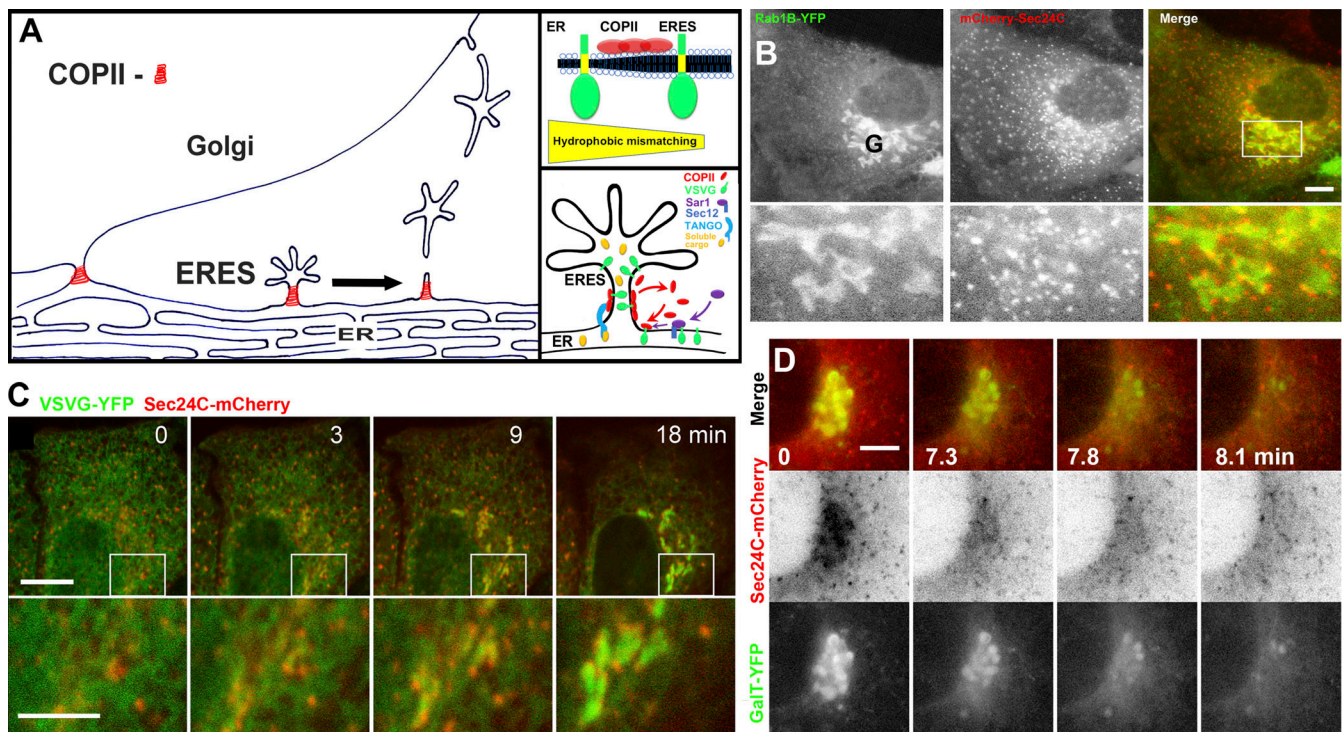
Figure 7. **Schematic representation for the localization and function of the COPII heterocomplex at the ER–ERES boundary: Support for direct ERES to Golgi transport. (A)** The localization and function of the COPII heterocomplex at the ER–ERES boundary. Main panel: COPII dynamically binds and establishes domains of collar-like elongated membranes that comprise a stable ER–ERES boundary. Cargo accumulates in COPII-free ERES membranes by passage through the COPII coated neck. Fission ensues to form Golgi bound COPII-deficient carriers. Top right: Hydrophobic mismatching between transmembrane domains of cargo proteins and surrounding lipids is essential for cargo sorting: Schematic representation demonstrating how bilayer thickness gradient from thinner ER to thicker ERES membranes drives cargo into ERES. Alleviation of hydrophobic mismatching of cargo transmembrane domains facilitates their concentration in ERES membranes by preventing their diffusion through the COPII neck back to the ER. Bottom right: A detailed model of the COPII cargo sorting machinery at the ER–ERES boundary. COPII is recruited exclusively at the ER adjacent to the COPII neck by Sec12 and Sar1-GTP and binds cargo via the Sec24 subunit. The COPII-cargo complex is driven toward ERES potentially by the abovementioned hydrophobic mismatch interactions. COPII coat disassembly initiated by Sar1-GTP hydrolysis releases the cargo at the distal ERES end of the COPII-coated neck. **(B)** Golgi-associated ERESs in living intact cells. The intracellular distribution of COPII subunit Sec24C-mCherry (red) and Rab1b-YFP were used here as a Golgi marker. A confocal image of the Huh7 cell coexpressing the Rab1-YFP (left, and green in merged image) and the COPII subunit Sec24C-mCherry (center, and red in merged image). Golgi apparatus marked by G. The frame showing the Golgi apparatus is enlarged threefold below. Scale bar = 5 μm. **(C)** Stable Golgi-associated ERES during cargo accumulation in Golgi apparatus. Time-lapse analysis of living cells coexpressing Sec24C-mCherry (red) and VSVG-YFP (green), showing an accumulation of cargo VSVG-YFP in Golgi membranes decorated with COPII-labeled domains. The area in white rectangles is magnified 3.3-fold on the bottom. Scale bars in top and bottom panels are 10 and 5 μm, respectively. **(D)** Golgi-associated ERESs disappear upon BFA-induced Golgi membranes blink-out. Representative images from a time-lapse sequence taken at 3-s intervals after addition of 5 μg/ml BFA to living cells coexpressing GalT-YFP (green, bottom) and Sec24C-mCherry (red and inverted, middle). Times are counted. Scale bar = 5 μm.

to carriers, and move to fuse with the Golgi are COPII-deficient. Our findings are consistent with several previously published studies. (i) The stationary and stable appearance of COPII-labeled domains (Hammond and Glick, 2000; Stephens et al., 2000; Westrate et al., 2020) challenges the role of COPII as a vesicle coat as it is absent from mobile carriers. Its apparent stability during cargo accumulation in adjacent ERESs is inconsistent with the expected COPII accumulation during the cargo selection-coupled coat assembly (Kuehn et al., 1998). (ii) The localization and function of COPII as a gatekeeper at the ER–ERES boundary is consistent with its emerging role in quality control (Ma et al., 2017; Mezzacasa and Helenius, 2002). (iii) Our model is compatible with the export mechanism proposed for large cargo molecules such as procollagen (Raote et al., 2020; Raote and Malhotra, 2019; Raote et al., 2018; Saito et al., 2009). Essentially, the localization of COPII to the ER–ERES

boundary is preempting the need for a variety of coat configurations to fit different cargo shapes and sizes. (iv) Our model explains the observations of early recruitment of COPI to anterograde transport carriers in close proximity to the ER (Bednarek et al., 1995; Orci et al., 1997; Presley et al., 2002; Scales et al., 1997; Stephens et al., 2000). As COPII occupies the ER–ERES boundary, COPI on ERES membranes may well be involved in the fission of the final transport carrier from the ERES, also more directly explaining why BFA, an inhibitor of the ARF1 GDP-to-GTP exchange factor, inhibits ER export. Undoubtedly, the core COPII proteins Sar1, Sec13/31, Sec23/24, Sec12, and Sec16 are essential for ER export. They are involved in recruiting and concentrating cargo at ERES. It is widely accepted that upon recruitment to ER membranes, COPII coat induces buds that eventually transform to spherical 60–70-nm vesicles (Zanetti et al., 2011; Barlowe and Helenius, 2016; Gomez-Navarro and

Shomron et al.
COPII defines the boundary between ER and EREs

Journal of Cell Biology   10 of 16
https://doi.org/10.1083/jcb.201907224

Miller, 2016; Aridor, 2018). COPII-coated vesicles were indeed observed in in vitro assays (Barlowe et al., 1994) and since then observed in other systems: in yeast (Mogelsvang et al., 2003), plants and algae (Donohoe et al., 2013; Staehelin and Kang, 2008), and mammalian cells (Zeuschner et al., 2006). However, doubts about the existence of COPII vesicles in mammalian cells persisted (Fromme and Schekman, 2005; Mironov et al., 2003; Mironov et al., 1997) and even increased over the years (McCaughey et al., 2019; Raote et al., 2017; Raote et al., 2018; Santos et al., 2015; Westrate et al., 2020). How can the COPII collar at the ER–ERES boundary act as a gatekeeper and concentrate cargo in ERES? We suggest two distinct and established driving forces that simultaneously facilitate cargo selection, entry, and concentration into ERESs. The first is based on the interaction of cargo protein with its surrounding membrane. It is widely accepted that an ER–Golgi–plasma membrane thinner-to-thicker gradient of membrane thickness is critical for targeting proteins in the secretory pathway (Sharpe et al., 2010). The transmembrane domain (TMD) of plasma membrane–destined cargo such as VSVG is longer than the average thickness of the ER membrane and thus hydrophobically mismatched with the thinner ER membrane. Alleviation of this mismatching can thermodynamically drive cargo membrane proteins' movement from the thinner ER into the thicker ERESs (Borgese, 2016). To this end, we demonstrated that stepwise shortening of the TMD of VSVG proportionally slows its accumulation and decreases its concentration in ERESs and the trans-Golgi network, thereby slowing its passage through the secretory pathway (Dejgaard et al., 2008; Dukhovny et al., 2009). Also, the cargo receptor Erv14 in yeast was shown to preferentially bind cargo with longer TMDs (Herzig et al., 2012). The membrane tension caused by mismatching may be locally restricted to the lipids surrounding the cargo TMD. Although it may not facilitate long-range cargo movement, it can stabilize the concentrating cargo population in the thicker ERES membrane (Dukhovny et al., 2009). The second mechanism for cargo entry into ERESs is the COPII-cargo export signal–specific interaction that directly mediates the selective concentration of cargo in ERESs (Balch et al., 1994; Campbell and Schekman, 1997; Kuehn et al., 1998; Nishimura and Balch, 1997). Membrane-bound COPII exchanges regularly with a cytosolic pool (Forster et al., 2006). COPII is recruited by and subsequently replaces Sec12 and Sar1, which reside in the ER membrane (Kurokawa et al., 2016). Here, we propose that the continuous addition of COPII at the ER side of the COPII domain results in an overall ER-to-ERES directional movement of the membrane-bound COPII coat. Thus, the COPII coat binds the cargo on the ER and releases it on the other side of the COPII-coated membrane collar.

Together, these mechanisms result in the capacity of the COPII complex to generate a selective and directed flux of cargo to the ERES. Our model allows the on-demand flexible and extensive proliferation of membranes to generate large ER-to-Golgi carriers (Presley et al., 1997). The recent idea of transport in nonvesicular tubular elements (tunnels) suggested by the Malhotra and Stephens laboratories is consistent with the localization of COPII reported here (Malhotra and Erlmann, 2015; Raote and Malhotra, 2019).

We and others have found COPI colocalizing with COPII and their sequential function in ER-to-Golgi transport (Lavoie et al., 1999; Scales et al., 1997). Based on our model placing COPII at the ER–ERES boundary, we propose that COPI binds cargo carriers already on ERES membranes and not at a later stage in the ER–Golgi intermediate compartment. This hypothesis is supported by a coincidental decrease of COPII and an increase of COPI on ER-to-Golgi carriers (Scales et al., 1997). Also, at the EM level, it was shown that cargo undergoes concentration only on ERES but not later (Balch et al., 1994). The idea that the ERGIC is essentially a COPI-coated anterograde carrier that buds en bloc from ERESs is not very different from the current concept of ERGIC. The juxtaposition of COPI-positive ERGIC and ERESs was also demonstrated (Ben-Tekaya et al., 2005). In this and other studies (Farhan et al., 2008; Shima et al., 1999), COPI-positive membranes are considered to be ERGIC that is adjacent yet physically separated from ERESs.

How to reconcile our hypothesis with previous data and models?
The genetic and protein–protein interactions data surrounding COPII-mediated ER cargo export are all entirely consistent with our model. What indeed conflicts with our data is the evidence for COPII vesicles from EM data (Zeuschner et al., 2006). The conventional vesicle coat model of COPII is based on ultrastructural studies of purified COPII components and artificial membranes (Béthune and Wieland, 2018; Mancias and Goldberg, 2008). These studies could not identify the function of COPII at the ER–ERES boundary as vesicle formation was analyzed in a cell-free system that cannot assign a precise intracellular localization to the process. The use of semi-permeable cells to reconstitute COPII vesicle formation may also have altered the fragile tubular–vesicular structure of the ERESs due to potentially destructive effects of the permeabilizing detergent on membranes. The concern that a substantial amount of data on COPII vesicles is indirect has been raised previously (Mironov, 2014; Mironov et al., 2003). Recent ultrastructural studies demonstrated and analyzed COPII-mediated tubular membrane structures (O'Donnell et al., 2011; Zanetti et al., 2013). These structures observed in vitro might correlate with the COPII collar in situ. Small round COPII vesicles (Donohoe et al., 2013; Staehelin and Kang, 2008; Zeuschner et al., 2006) may be more common in lower organisms, yet are the exception rather than the rule in mammalian cells. Future work using ultrafast super-resolution microscopy could clarify this point as there should be no principal obstacle to visualize 50–100-nm vesicles labeled with fluorescent cargo or coat.

The data presented here lay the foundation for an alternative model of how, where, and when the COPII complex orchestrates the functions of the ERES domain. This model is of major significance as it allows a better understanding of protein retention mechanisms and export from the ER in heath and disease.

Materials and methods
Reagents and constructs
All reagents were purchased from Sigma-Aldrich unless otherwise stated. Human Sec24B was subcloned into pmCherry-C1

(Clontech) using *Sal*I and *Bgl*II restriction sites and verified by sequencing. Human Sec24C was subcloned into pmCherry-C1 or pEYFP-C1 (Clontech) using *Xho*I and *Sac*II restriction sites and verified by sequencing. Human Rab1B was cloned into pEGFP-C1 (Clontech) using *Xho*I and *Bam*HI restriction sites and verified by sequencing. ss-mCherry (mCherry with the signal sequence from hen-egg-lysozyme). YFP-VSVGtsO45 was prepared as described elsewhere (Ward et al., 2001). GalT-YFP was prepared as described elsewhere (Zaal et al., 1999). GFP-CFTR and CFTRΔ508-GFP were a kind gift from R. Kopito (Stanford University, Stanford, CA). Rab1b was prepared as described elsewhere (Nevo-Yassaf et al., 2012). Reticulon-GFP was a kind gift from T. Rapoport (Harvard University, Boston, MA). Carboxypeptidase E was a kind gift from R. Harbesfeld (TAU, Tel-Aviv, Israel). Sec24B V932R mutant was prepared using the Quick-Change kit from Stratagene. The primer used for the PCR reaction was 5′-CAAGAAAAATTGGGTTTGAAGCTAGAATGAGAATAAGGTGTACTAAAGG-3′.

Cell culture, and transfections
COS-7, Huh7, or HeLa cells were grown at 37°C in a 5% CO_2-humidified atmosphere. Cell cultures were maintained in DMEM supplemented with 10% (vol/vol) fetal bovine serum and penicillin and streptomycin (Biological Industries). A final concentration of 1% (vol/vol) nonessential amino acids was added to the Huh7 cells culture media. Polyethyleneimine MAX transfection reagent (Thermo Fisher Scientific) was used following the manufacturer's protocols for plasmid DNA transfections of subconfluent COS7 and Huh7 cells. Confocal laser scanning microscopy experiments were performed 18–24 h after transfection.

CRISPR-Cas12a–assisted PCR tagging of SEC13 with mCherry
Endogenous SEC13 was tagged at the C terminus with mCherry using the PCR-based method described by Fueller et al. (2020). PCR was performed on plasmid pMaCTag-P13 (Addgene; #120024), kindly provided by Marius Lemberg (Zentrum für Molekulare Biologie der Universität Heidelberg, Heidelberg, Germany), using oligos M1_SEC13, 5′-GTTGATGGGCAGTGGGTGTGCATCAGTGATGTCAACAAGGGCCAGGGCTCCGTATCAGCATCAGTGACAGAGGGCCAGCAGAACGAGCAGTCAGGTGGAGGAGGTAGTG-3′ and M2_Sec13_, 5′-CAGGAAGGGGCAGTCCTGGAGCTGGCGGGTGGGGAGCCAGGCCCCACCTGTCTTGAAAAAAAGCAGAACGAGCAGTGACAAATCTACAAGAGTAGAAATTAGCTAGCTGCATCGGTACC-3′. Cells were transfected with purified PCR product, and enAsCas12a was a gift from Keith Joung and Benjamin Kleinstiver (Molecular Pathology Unit, Massachusetts General Hospital, Charlestown, MA; Addgene; #107941; Kleinstiver et al., 2019) and selected for 7 d with puromycin. After that, cells were FACS-sorted in four different fractions that were analyzed for proper mCherry localization. The fraction with the lowest intensity contained mainly cells with mCherry staining ERES. Single-cell clones were isolated and characterized. One representative clone, L6, heterozygous for the tagged insertion, was chosen for further analysis. The amino acid sequence at the fusion site is SVTEGQQNEQSGGGGSGGGGS*VSKGEEDNMAIIKE* (underlined, SEC13; italics, mCherry; SGGGGS GGGGS, inserted linker).

Live-cell microscopy
Cells were imaged in DMEM without phenol red but with supplements, including 20 mM Hepes, pH 7.4. Transfection and imaging were performed in a 35-mm glass-bottomed microwell dish (MatTek) or glass coverslips. A Zeiss LSM710 or LSM800 confocal laser-scanning microscope was used (Carl Zeiss MicroImaging). Fluorescence emissions resulting from 405-nm excitation for CFP, 488-nm excitation for GFP, and 543-nm excitation for mCherry were detected using filter sets supplied by the manufacturer. The confocal and time-lapse images were captured using a Plan-Apochromat 63× 1.4-NA objective (Carl Zeiss MicroImaging). The temperature on the microscope stage was held stable during time-lapse sessions using an electronic temperature-controlled airstream incubator. Images and videos were generated and analyzed using the Zeiss LSM Zen software and National Institutes of Health Image and ImageJ software (W. Rasband, National Institutes of Health, Bethesda, MD). High-frequency images were captured using a Nikon Ti microscope equipped with a Yokogawa CSU X-1 spinning disc, controlled by Andor IQ2 software, or a spinning disk confocal unit (Yokogawa Electric; CSU-X1) attached to an Axio Observer Z1 microscope (Carl Zeiss).

Confocal lasers scanning microscopy, time-lapse imaging, and FRAP analyses
For FRAP measurements, a 63× 1.4-NA Plan-Apochromat objective was used on an inverted LSM800 system. Photobleaching of GFP was performed using four to six rapid scans with the laser at full power. Pre- and post-bleach images were captured at 0.5- to 3-s intervals, using low laser intensity. Fluorescence recovery in the bleached region during the time series was quantified using LSM Zen software (Carl Zeiss MicroImaging). For presentation purposes, 16-bit confocal images were exported in TIFF, and their contrast and brightness were optimized in Adobe Photoshop software or ImageJ. The characteristic fluorescence recovery time (τ) values for membrane-bound Sec24b turnover were calculated from the photobleaching data by fitting the data to a simple exponential equation using Kalaidagraph software (Synergy Software),

$$y = Mf \cdot \left(1 - e^{-kt}\right),$$

where *Mf* is mobile fraction. R^2 = 0.98 and 0.97 for WT and mutant, respectively.

Immunofluorescence antibody staining
Cells cultured on coverslips were fixed at room temperature in a mixture of 2% paraformaldehyde–PBS for 10 min, then washed three times with 1× PBS + 3% FCS. Cells were permeabilized and labeled simultaneously by incubation with appropriate primary antibodies: anti-Sec24C (4 µg/ml; Abcam; catalog no. Ab122635) and 0.01% saponin at room temperature for 1 h. Cells were washed three times with 1× PBS for 5 min at room temperature and incubated for 1 h at room temperature with appropriate Cy3 secondary antibodies (dilution, 1:200; Jackson ImmunoResearch) and 0.1% saponin. Images were acquired using a Zeiss Pascal confocal laser-scanning microscope as described above or an Axio Observer Z1 fluorescence microscope (Carl Zeiss). For

Sec13 detection, a rabbit anti-SEC13 antibody was used (1:1,000; R&D Systems; MAB9055-SP).

EM

COS7 cells expressing Sec23-GFP and VSVG-Scarlet under BFA/Noc treatment were fixed 30 min after the shift to permissive temperature for immuno-EM (Beznoussenko et al., 2014) Briefly, cells were fixed with 1% glutaraldehyde in Hepes, pH 7.0, post-fixed in reduced OsO_4 for 2 h, washed, treated with 0.3% thiocarbohydrazide for 30 min, and then, after the washout, with 1% OsO_4 for 1 h (sometimes treatment with thiocarbohydrazide and OsO_4 was done three times) followed by dehydration and embedding in Epon-812. Cells were then incubated with polyclonal anti-GFP antibody (Abcam; UK AB6556) for 2 h and subsequently with anti-rabbit Fab' fragment nanogold conjugates (Nanoprobes; #2004) for 2 h, enhanced with the GoldEnhance kit (NanoProbes) according to the manufacturer's instruction. Epon embedding and sectioning of the gold-labeled cells, two-step EM tomography, and 3D reconstruction were performed as reported earlier (Beznoussenko et al., 2014; Beznoussenko et al., 2016). Briefly, an ultratome (Leica AFS; Leica Microsystems) was used to cut 60-nm serial thin sections and 200-nm serial semi-thick sections. Sections were collected onto 1% Formvar films adhered to slot grids. Both sides of the grids were labeled with fiduciary 10-nm colloidal gold (British Biocell International). Sections were analyzed under a Tecnai-12 electron microscope (Thermo Fisher Scientific) equipped with Analysis software.

Immunoprecipitation and Western blot analysis

24 h following transfection, cells were washed with PBS and solubilized in lysis buffer (50 mm Tris-HCl, pH 7.4, 1% NP-40, 0.25% sodium deoxycholate, 150 mm NaCl, and 1 mm EDTA) containing protease inhibitor cocktail (Sigma-Aldrich). Extracts were clarified by centrifugation at 12,000 g for 15 min at 4°C. Following SDS-PAGE separation, proteins were transferred onto nitrocellulose membranes and blocked with 5% low-fat milk. Membranes were incubated with specific primary antibodies, washed with PBS containing 0.001% Tween-20, and incubated with the appropriate horseradish peroxidase–conjugated secondary antibody. After washing in PBS containing 0.001% Tween-20, membranes were subjected to enhanced chemiluminescence detection analysis. For immunoprecipitation analysis, cells were solubilized in lysis buffer (see above). Cell lysates were incubated with the specific antibody for 2–3 h, at 4°C, followed by 3–18 h rotated incubation with protein A/G agarose beads (Santa Cruz Biotechnology) at 4°C. Beads were collected by slow centrifugation, washed four times with lysis buffer, and analyzed by SDS-PAGE followed by detection with a specific antibody. Immunoprecipitation from the medium was performed similarly.

Antibodies used were Sec31-mouse anti-SEC31A antibody (Becton Dickinson; 61235), actin-rabbit anti-actin (Abcam; ab8227), mCherry-rabbit anti-mCherry antibody (Abcam; 167453), VSVG-mouse anti-VSVG antibody (8G5F11; Kerafast; EB0010), GFP-rabbit anti-GFP (Invitrogen; A-11122), and tubulin-mouse anti-αtubulin (Sigma-Aldrich; T6199).

Chemiluminescence was recorded with an Imager LAS4000 mini (FujiFilm Live Science USA).

Online supplemental material

Fig. S1 illustrates characterization of HeLa cells with Sec13 endogenously tagged with mCherry, using immunofluorescence microscopy and Western blot analysis. Fig. S2 shows the structure and function of ER exit sites in BFA/Noc-treated cells. Fig. S3 shows that the Sec24BV932R mutant interacts with VSVG. Fig. S4 displays colocalization to and translocation from ERESs of COPI-coated membranes. Video 1 shows a time-lapse of VSVG-EGFP trafficking in Sec13-mCherry CRSPR/CAS12 knock-in HeLa cells. Video 2 shows COS7 cell co-expressing VSVG-YFP and the COPII subunit Sec24C-mCherry after shift to permissive temperature (32°C). Video 3 shows microtubule plus-end polymerization in COS7 co-expressing EB3-GFP and the COPII subunit Sec24C-mCherry. Video 4 shows cargo accumulation and fission of carriers from ERESs in COS7 cells co-expressing COPII subunit Sec24C-mCherry and VSVG-YFP. Video 5, Video 6, Video 7, and Video 8 show cargo accumulation and carrier fission in a single ERES. Video 9 shows photobleaching of the Golgi to expose ER to Golgi carrier life history. Video 10 shows Rab1b localizes with VSVG-YFP cargo throughout the Life history of ER-to-Golgi carriers. Video 11 and Video 12 show COPII labeled membranes separate ER and ERES membranes in BFA/nocodazole treated cells. Video 13 shows that ERESs are connected to the ER in BFA/Noc treated cells. Video 14 shows cargo and membrane accumulation in a single exit site under BFA/Nocodazole treatment. Video 15 shows COPII-mediated cargo sorting in ERESs of BFA/Nocodazole-treated COS7 cells. Video 16 shows that Golgi-associated ERESs disappear upon BFA-induced Golgi membranes blink-out. Video 17 shows translocation from ERESs of COPI coated membranes in e-COP-YFP expressing LDLF cells.

JCB logo

References

Aridor, M. 2018. COPII gets in shape: Lessons derived from morphological aspects of early secretion. *Traffic.* 19:823–839. https://doi.org/10.1111/tra.12603

Balch, W.E., J.M. McCaffery, H. Plutner, and M.G. Farquhar. 1994. Vesicular stomatitis virus glycoprotein is sorted and concentrated during export from the endoplasmic reticulum. *Cell.* 76:841–852. https://doi.org/10.1016/0092-8674(94)90359-X

Barlowe, C., and A. Helenius. 2016. Cargo Capture and Bulk Flow in the Early Secretory Pathway. *Annu. Rev. Cell Dev. Biol.* 32:197–222. https://doi.org/10.1146/annurev-cellbio-111315-125016

Barlowe, C., L. Orci, T. Yeung, M. Hosobuchi, S. Hamamoto, N. Salama, M.F. Rexach, M. Ravazzola, M. Amherdt, and R. Schekman. 1994. COPII: a membrane coat formed by Sec proteins that drive vesicle budding from the endoplasmic reticulum. *Cell.* 77:895–907. https://doi.org/10.1016/0092-8674(94)90138-4

Bednarek, S.Y., M. Ravazzola, M. Hosobuchi, M. Amherdt, A. Perrelet, R. Schekman, and L. Orci. 1995. COPI- and COPII-coated vesicles bud directly from the endoplasmic reticulum in yeast. *Cell.* 83:1183–1196. https://doi.org/10.1016/0092-8674(95)90144-2

Ben-Tekaya, H., K. Miura, R. Pepperkok, and H.P. Hauri. 2005. Live imaging of bidirectional traffic from the ERGIC. *J. Cell Sci.* 118:357–367. https://doi.org/10.1242/jcs.01615

Béthune, J., and F.T. Wieland. 2018. Assembly of COPI and COPII Vesicular Coat Proteins on Membranes. *Annu. Rev. Biophys.* 47:63–83. https://doi.org/10.1146/annurev-biophys-070317-033259

Beznoussenko, G.V., S. Parashuraman, R. Rizzo, R. Polishchuk, O. Martella, D. Di Giandomenico, A. Fusella, A. Spaar, M. Sallese, M.G. Capestrano, et al. 2014. Transport of soluble proteins through the Golgi occurs by diffusion via continuities across cisternae. *eLife.* 3:e02009. https://doi.org/10.7554/eLife.02009

Beznoussenko, G.V., A. Ragnini-Wilson, C. Wilson, and A.A. Mironov. 2016. Three-dimensional and immune electron microscopic analysis of the secretory pathway in Saccharomyces cerevisiae. *Histochem. Cell Biol.* 146:515–527. https://doi.org/10.1007/s00418-016-1483-y

Blum, R., D.J. Stephens, and I. Schulz. 2000. Lumenal targeted GFP, used as a marker of soluble cargo, visualises rapid ERGIC to Golgi traffic by a tubulo-vesicular network. *J. Cell Sci.* 113:3151–3159.

Boncompain, G., S. Divoux, N. Gareil, H. de Forges, A. Lescure, L. Latreche, V. Mercanti, F. Jollivet, G. Raposo, and F. Perez. 2012. Synchronization of secretory protein traffic in populations of cells. *Nat. Methods.* 9:493–498. https://doi.org/10.1038/nmeth.1928

Borgese, N. 2016. Getting membrane proteins on and off the shuttle bus between the endoplasmic reticulum and the Golgi complex. *J. Cell Sci.* 129:1537–1545. https://doi.org/10.1242/jcs.183335

Campbell, J.L., and R. Schekman. 1997. Selective packaging of cargo molecules into endoplasmic reticulum-derived COPII vesicles. *Proc. Natl. Acad. Sci. USA.* 94:837–842. https://doi.org/10.1073/pnas.94.3.837

Dejgaard, S.Y., A. Murshid, A. Erman, O. Kizilay, D. Verbich, R. Lodge, K. Dejgaard, T.B. Ly-Hartig, R. Pepperkok, J.C. Simpson, and J.F. Presley. 2008. Rab18 and Rab43 have key roles in ER-Golgi trafficking. *J. Cell Sci.* 121:2768–2781. https://doi.org/10.1242/jcs.021808

Dolinsky, T.J., P. Czodrowski, H. Li, J.E. Nielsen, J.H. Jensen, G. Klebe, and N.A. Baker. 2007. PDB2PQR: expanding and upgrading automated preparation of biomolecular structures for molecular simulations. *Nucleic Acids Res.* 35(Web Server):W522-5. https://doi.org/10.1093/nar/gkm276

Donohoe, B.S., B.H. Kang, M.J. Gerl, Z.R. Gergely, C.M. McMichael, S.Y. Bednarek, and L.A. Staehelin. 2013. Cis-Golgi cisternal assembly and biosynthetic activation occur sequentially in plants and algae. *Traffic.* 14:551–567. https://doi.org/10.1111/tra.12052

Dukhovny, A., A. Papadopulos, and K. Hirschberg. 2008. Quantitative live-cell analysis of microtubule-uncoupled cargo-protein sorting in the ER. *J. Cell Sci.* 121:865–876. https://doi.org/10.1242/jcs.019463

Dukhovny, A., Y. Yaffe, J. Shepshelovitch, and K. Hirschberg. 2009. The length of cargo-protein transmembrane segments drives secretory transport by facilitating cargo concentration in export domains. *J. Cell Sci.* 122:1759–1767. https://doi.org/10.1242/jcs.039339

Fan, J.Y., J. Roth, and C. Zuber. 2003. Ultrastructural analysis of transitional endoplasmic reticulum and pre-Golgi intermediates: a highway for cars and trucks. *Histochem. Cell Biol.* 120:455–463. https://doi.org/10.1007/s00418-003-0597-1

Farhan, H., V. Reiterer, V.M. Korkhov, J.A. Schmid, M. Freissmuth, and H.H. Sitte. 2007. Concentrative export from the endoplasmic reticulum of the gamma-aminobutyric acid transporter 1 requires binding to SEC24D. *J. Biol. Chem.* 282:7679–7689. https://doi.org/10.1074/jbc.M609720200

Farhan, H., M. Weiss, K. Tani, R.J. Kaufman, and H.P. Hauri. 2008. Adaptation of endoplasmic reticulum exit sites to acute and chronic increases in cargo load. *EMBO J.* 27:2043–2054. https://doi.org/10.1038/emboj.2008.136

Forster, R., M. Weiss, T. Zimmermann, E.G. Reynaud, F. Verissimo, D.J. Stephens, and R. Pepperkok. 2006. Secretory cargo regulates the turnover of COPII subunits at single ER exit sites. *Curr. Biol.* 16:173–179. https://doi.org/10.1016/j.cub.2005.11.076

Fromme, J.C., and R. Schekman. 2005. COPII-coated vesicles: flexible enough for large cargo? *Curr. Opin. Cell Biol.* 17:345–352. https://doi.org/10.1016/j.ceb.2005.06.004

Fueller, J., K. Herbst, M. Meurer, K. Gubicza, B. Kurtulmus, J.D. Knopf, D. Kirrmaier, B.C. Buchmuller, G. Pereira, M.K. Lemberg, and M. Knop. 2020. CRISPR-Cas12a-assisted PCR tagging of mammalian genes. *J. Cell Biol.* 219:e201910210. https://doi.org/10.1083/jcb.201910210

Gomez-Navarro, N., and E. Miller. 2016. Protein sorting at the ER-Golgi interface. *J. Cell Biol.* 215:769–778. https://doi.org/10.1083/jcb.201610031

Gorur, A., L. Yuan, S.J. Kenny, S. Baba, K. Xu, and R. Schekman. 2017. COPII-coated membranes function as transport carriers of intracellular procollagen I. *J. Cell Biol.* 216:1745–1759. https://doi.org/10.1083/jcb.201702135

Griffiths, G. 2000. Gut thoughts on the Golgi complex. *Traffic.* 1:738–745. https://doi.org/10.1034/j.1600-0854.2000.010906.x

Hammond, A.T., and B.S. Glick. 2000. Dynamics of transitional endoplasmic reticulum sites in vertebrate cells. *Mol. Biol. Cell.* 11:3013–3030. https://doi.org/10.1091/mbc.11.9.3013

Herzig, Y., H.J. Sharpe, Y. Elbaz, S. Munro, and M. Schuldiner. 2012. A systematic approach to pair secretory cargo receptors with their cargo suggests a mechanism for cargo selection by Erv14. *PLoS Biol.* 10:e1001329. https://doi.org/10.1371/journal.pbio.1001329

Hirschberg, K., C.M. Miller, J. Ellenberg, J.F. Presley, E.D. Siggia, R.D. Phair, and J. Lippincott-Schwartz. 1998. Kinetic analysis of secretory protein traffic and characterization of golgi to plasma membrane transport intermediates in living cells. *J. Cell Biol.* 143:1485–1503. https://doi.org/10.1083/jcb.143.6.1485

Kirk, S.J., and T.H. Ward. 2007. COPII under the microscope. *Semin. Cell Dev. Biol.* 18:435–447. https://doi.org/10.1016/j.semcdb.2007.07.007

Kleinstiver, B.P., A.A. Sousa, R.T. Walton, Y.E. Tak, J.Y. Hsu, K. Clement, M.M. Welch, J.E. Horng, J. Malagon-Lopez, I. Scarfò, et al. 2019. Engineered CRISPR-Cas12a variants with increased activities and improved targeting ranges for gene, epigenetic and base editing. *Nat. Biotechnol.* 37:276–282. https://doi.org/10.1038/s41587-018-0011-0

Klumperman, J., A. Schweizer, H. Clausen, B.L. Tang, W. Hong, V. Oorschot, and H.P. Hauri. 1998. The recycling pathway of protein ERGIC-53 and dynamics of the ER-Golgi intermediate compartment. *J. Cell Sci.* 111:3411–3425.

Kuehn, M.J., J.M. Herrmann, and R. Schekman. 1998. COPII-cargo interactions direct protein sorting into ER-derived transport vesicles. *Nature.* 391:187–190. https://doi.org/10.1038/34438

Kurokawa, K., Y. Suda, and A. Nakano. 2016. Sar1 localizes at the rims of COPII-coated membranes in vivo. *J. Cell Sci.* 129:3231–3237. https://doi.org/10.1242/jcs.189423

Lavoie, C., J. Paiement, M. Dominguez, L. Roy, S. Dahan, J.N. Gushue, and J.J. Bergeron. 1999. Roles for alpha(2)p24 and COPI in endoplasmic reticulum cargo exit site formation. *J. Cell Biol.* 146:285–299. https://doi.org/10.1083/jcb.146.2.285

Lee, C., and J. Goldberg. 2010. Structure of coatomer cage proteins and the relationship among COPI, COPII, and clathrin vesicle coats. *Cell.* 142:123–132. https://doi.org/10.1016/j.cell.2010.05.030

Lippincott-Schwartz, J., L.C. Yuan, J.S. Bonifacino, and R.D. Klausner. 1989. Rapid redistribution of Golgi proteins into the ER in cells treated with brefeldin A: evidence for membrane cycling from Golgi to ER. *Cell.* 56:801–813. https://doi.org/10.1016/0092-8674(89)90685-5

London, N., B. Raveh, E. Cohen, G. Fathi, and O. Schueler-Furman. 2011. Rosetta FlexPepDock web server--high resolution modeling of peptide-protein interactions. *Nucleic Acids Res.* 39(suppl 2):W249-53. https://doi.org/10.1093/nar/gkr431

Ma, W., E. Goldberg, and J. Goldberg. 2017. ER retention is imposed by COPII protein sorting and attenuated by 4-phenylbutyrate. *eLife*. 6:e26624. https://doi.org/10.7554/eLife.26624

Malhotra, V., and P. Erlmann. 2015. The pathway of collagen secretion. *Annu. Rev. Cell Dev. Biol.* 31:109–124. https://doi.org/10.1146/annurev-cellbio-100913-013002

Malkus, P., F. Jiang, and R. Schekman. 2002. Concentrative sorting of secretory cargo proteins into COPII-coated vesicles. *J. Cell Biol.* 159:915–921. https://doi.org/10.1083/jcb.200208074

Mancias, J.D., and J. Goldberg. 2008. Structural basis of cargo membrane protein discrimination by the human COPII coat machinery. *EMBO J.* 27:2918–2928. https://doi.org/10.1038/emboj.2008.208

McCaughey, J., N.L. Stevenson, S. Cross, and D.J. Stephens. 2019. ER-to-Golgi trafficking of procollagen in the absence of large carriers. *J. Cell Biol.* 218:929–948. https://doi.org/10.1083/jcb.201806035

Mezzacasa, A., and A. Helenius. 2002. The transitional ER defines a boundary for quality control in the secretion of tsO45 VSV glycoprotein. *Traffic*. 3:833–849. https://doi.org/10.1034/j.1600-0854.2002.31108.x

Mironov, A.A. 2014. ER-Golgi transport could occur in the absence of COPII vesicles. *Nat. Rev. Mol. Cell Biol.* 15:1. https://doi.org/10.1038/nrm3588-c1

Mironov, A.A., and G.V. Beznoussenko. 2019. Models of Intracellular Transport: Pros and Cons. *Front. Cell Dev. Biol.* 7:146. https://doi.org/10.3389/fcell.2019.00146

Mironov, A.A., P. Weidman, and A. Luini. 1997. Variations on the intracellular transport theme: maturing cisternae and trafficking tubules. *J. Cell Biol.* 138:481–484. https://doi.org/10.1083/jcb.138.3.481

Mironov, A.A., A.A. Mironov Jr., G.V. Beznoussenko, A. Trucco, P. Lupetti, J.D. Smith, W.J. Geerts, A.J. Koster, K.N. Burger, M.E. Martone, et al. 2003. ER-to-Golgi carriers arise through direct en bloc protrusion and multistage maturation of specialized ER exit domains. *Dev. Cell*. 5:583–594. https://doi.org/10.1016/S1534-5807(03)00294-6

Mogelsvang, S., N. Gomez-Ospina, J. Soderholm, B.S. Glick, and L.A. Staehelin. 2003. Tomographic evidence for continuous turnover of Golgi cisternae in Pichia pastoris. *Mol. Biol. Cell*. 14:2277–2291. https://doi.org/10.1091/mbc.e02-10-0697

Nevo-Yassaf, I., Y. Yaffe, M. Asher, O. Ravid, S. Eizenberg, Y.I. Henis, Y. Nahmias, K. Hirschberg, and E.H. Sklan. 2012. Role for TBC1D20 and Rab1 in hepatitis C virus replication via interaction with lipid droplet-bound nonstructural protein 5A. *J. Virol.* 86:6491–6502. https://doi.org/10.1128/JVI.00496-12

Nishimura, N., and W.E. Balch. 1997. A di-acidic signal required for selective export from the endoplasmic reticulum. *Science*. 277:556–558. https://doi.org/10.1126/science.277.5325.556

O'Donnell, J., K. Maddox, and S. Stagg. 2011. The structure of a COPII tubule. *J. Struct. Biol.* 173:358–364. https://doi.org/10.1016/j.jsb.2010.09.002

Orci, L., M. Stamnes, M. Ravazzola, M. Amherdt, A. Perrelet, T.H. Söllner, and J.E. Rothman. 1997. Bidirectional transport by distinct populations of COPI-coated vesicles. *Cell*. 90:335–349. https://doi.org/10.1016/S0092-8674(00)80341-4

Pavelka, M., and A. Ellinger. 1993. Early and late transformations occurring at organelles of the Golgi area under the influence of brefeldin A: an ultrastructural and lectin cytochemical study. *J. Histochem. Cytochem.* 41:1031–1042. https://doi.org/10.1177/41.7.8515046

Peotter, J., W. Kasberg, I. Pustova, and A. Audhya. 2019. COPII-mediated trafficking at the ER/ERGIC interface. *Traffic*. 20:491–503. https://doi.org/10.1111/tra.12654

Pettersen, E.F., T.D. Goddard, C.C. Huang, G.S. Couch, D.M. Greenblatt, E.C. Meng, and T.E. Ferrin. 2004. UCSF Chimera--a visualization system for exploratory research and analysis. *J. Comput. Chem.* 25:1605–1612. https://doi.org/10.1002/jcc.20084

Presley, J.F., N.B. Cole, T.A. Schroer, K. Hirschberg, K.J.M. Zaal, and J. Lippincott-Schwartz. 1997. ER-to-Golgi transport visualized in living cells. *Nature*. 389:81–85. https://doi.org/10.1038/38001

Presley, J.F., T.H. Ward, A.C. Pfeifer, E.D. Siggia, R.D. Phair, and J. Lippincott-Schwartz. 2002. Dissection of COPI and Arf1 dynamics in vivo and role in Golgi membrane transport. *Nature*. 417:187–193. https://doi.org/10.1038/417187a

Rambourg, A., and Y. Clermont. 1992. Three-dimensional structure of cytidine monophosphatase reactive trans-Golgi elements in spinal ganglion cells of the rat. *Anat. Rec.* 232:25–35. https://doi.org/10.1002/ar.1092320104

Rambourg, A., Y. Clermont, C.L. Jackson, and F. Képès. 1995a. Effects of brefeldin A on the three-dimensional structure of the Golgi apparatus in a sensitive strain of Saccharomyces cerevisiae. *Anat. Rec.* 241:1–9. https://doi.org/10.1002/ar.1092410102

Rambourg, A., Y. Clermont, L. Ovtracht, and F. Képès. 1995b. Three-dimensional structure of tubular networks, presumably Golgi in nature, in various yeast strains: a comparative study. *Anat. Rec.* 243:283–293. https://doi.org/10.1002/ar.1092430302

Raote, I., and V. Malhotra. 2019. Protein transport by vesicles and tunnels. *J. Cell Biol.* 218:737–739. https://doi.org/10.1083/jcb.201811073

Raote, I., M. Ortega Bellido, M. Pirozzi, C. Zhang, D. Melville, S. Parashuraman, T. Zimmermann, and V. Malhotra. 2017. TANGO1 assembles into rings around COPII coats at ER exit sites. *J. Cell Biol.* 216:901–909. https://doi.org/10.1083/jcb.201608080

Raote, I., M. Ortega-Bellido, A.J. Santos, O. Foresti, C. Zhang, M.F. Garcia-Parajo, F. Campelo, and V. Malhotra. 2018. TANGO1 builds a machine for collagen export by recruiting and spatially organizing COPII, tethers and membranes. *eLife*. 7:e32723. https://doi.org/10.7554/eLife.32723

Raote, I., M. Chabanon, N. Walani, M. Arroyo, M.F. Garcia-Parajo, V. Malhotra, and F. Campelo. 2020. A physical mechanism of TANGO1-mediated bulky cargo export. *eLife*. 9:e59426. https://doi.org/10.7554/eLife.59426

Sáenz, J.B., W.J. Sun, J.W. Chang, J. Li, B. Bursulaya, N.S. Gray, and D.B. Haslam. 2009. Golgicide A reveals essential roles for GBF1 in Golgi assembly and function. *Nat. Chem. Biol.* 5:157–165. https://doi.org/10.1038/nchembio.144

Saito, K., M. Chen, F. Bard, S. Chen, H. Zhou, D. Woodley, R. Polischuk, R. Schekman, and V. Malhotra. 2009. TANGO1 facilitates cargo loading at endoplasmic reticulum exit sites. *Cell*. 136:891–902. https://doi.org/10.1016/j.cell.2008.12.025

Saito, K., K. Yamashiro, Y. Ichikawa, P. Erlmann, K. Kontani, V. Malhotra, and T. Katada. 2011. cTAGE5 mediates collagen secretion through interaction with TANGO1 at endoplasmic reticulum exit sites. *Mol. Biol. Cell*. 22:2301–2308. https://doi.org/10.1091/mbc.e11-02-0143

Santos, A.J., I. Raote, M. Scarpa, N. Brouwers, and V. Malhotra. 2015. TANGO1 recruits ERGIC membranes to the endoplasmic reticulum for procollagen export. *eLife*. 4:e10982. https://doi.org/10.7554/eLife.10982

Scales, S.J., R. Pepperkok, and T.E. Kreis. 1997. Visualization of ER-to-Golgi transport in living cells reveals a sequential mode of action for COPII and COPI. *Cell*. 90:1137–1148. https://doi.org/10.1016/S0092-8674(00)80379-7

Schindler, R., C. Itin, M. Zerial, F. Lottspeich, and H.P. Hauri. 1993. ERGIC-53, a membrane protein of the ER-Golgi intermediate compartment, carries an ER retention motif. *Eur. J. Cell Biol.* 61:1–9.

Sesso, A., F.P. de Faria, E.S. Iwamura, and H. Corrêa. 1994. A three-dimensional reconstruction study of the rough ER-Golgi interface in serial thin sections of the pancreatic acinar cell of the rat. *J. Cell Sci.* 107:517–528.

Sharpe, H.J., T.J. Stevens, and S. Munro. 2010. A comprehensive comparison of transmembrane domains reveals organelle-specific properties. *Cell*. 142:158–169. https://doi.org/10.1016/j.cell.2010.05.037

Shima, D.T., S.J. Scales, T.E. Kreis, and R. Pepperkok. 1999. Segregation of COPI-rich and anterograde-cargo-rich domains in endoplasmic-reticulum-to-Golgi transport complexes. *Curr. Biol.* 9:821–824. https://doi.org/10.1016/S0960-9822(99)80365-0

Staehelin, L.A., and B.H. Kang. 2008. Nanoscale architecture of endoplasmic reticulum export sites and of Golgi membranes as determined by electron tomography. *Plant Physiol.* 147:1454–1468. https://doi.org/10.1104/pp.108.120618

Stephens, D.J., N. Lin-Marq, A. Pagano, R. Pepperkok, and J.P. Paccaud. 2000. COPI-coated ER-to-Golgi transport complexes segregate from COPII in close proximity to ER exit sites. *J. Cell Sci.* 113:2177–2185.

Wang, X., J. Matteson, Y. An, B. Moyer, J.S. Yoo, S. Bannykh, I.A. Wilson, J.R. Riordan, and W.E. Balch. 2004. COPII-dependent export of cystic fibrosis transmembrane conductance regulator from the ER uses a di-acidic exit code. *J. Cell Biol.* 167:65–74. https://doi.org/10.1083/jcb.200401035

Ward, T.H., R.S. Polishchuk, S. Caplan, K. Hirschberg, and J. Lippincott-Schwartz. 2001. Maintenance of Golgi structure and function depends on the integrity of ER export. *J. Cell Biol.* 155:557–570. https://doi.org/10.1083/jcb.200107045

Wendeler, M.W., J.P. Paccaud, and H.P. Hauri. 2007. Role of Sec24 isoforms in selective export of membrane proteins from the endoplasmic reticulum. *EMBO Rep.* 8:258–264. https://doi.org/10.1038/sj.embor.7400893

Westrate, L.M., M.J. Hoyer, M.J. Nash, and G.K. Voeltz. 2020. Vesicular and uncoated Rab1-dependent cargo carriers facilitate ER to Golgi transport. *J. Cell Sci.* 133:jcs239814. https://doi.org/10.1242/jcs.239814

Yonemura, Y., X. Li, K. Muller, A. Kramer, P. Atigbire, T. Mentrup, T. Feuerhake, T. Kroll, O. Shomron, R. Nohl, et al. 2016. Inhibition of cargo

export at ER-exit sites and the trans-Golgi network by the secretion inhibitor FLI-06. *J. Cell Sci.* 129:3868–3877.

Yuan, L., S.J. Kenny, J. Hemmati, K. Xu, and R. Schekman. 2018. TANGO1 and SEC12 are copackaged with procollagen I to facilitate the generation of large COPII carriers. *Proc. Natl. Acad. Sci. USA.* 115:E12255–E12264. https://doi.org/10.1073/pnas.1814810115

Zaal, K.J., C.L. Smith, R.S. Polishchuk, N. Altan, N.B. Cole, J. Ellenberg, K. Hirschberg, J.F. Presley, T.H. Roberts, E. Siggia, et al. 1999. Golgi membranes are absorbed into and reemerge from the ER during mitosis. *Cell.* 99:589–601. https://doi.org/10.1016/S0092-8674(00)81548-2

Zanetti, G., K.B. Pahuja, S. Studer, S. Shim, and R. Schekman. 2011. COPII and the regulation of protein sorting in mammals. *Nat. Cell Biol.* 14:20–28. https://doi.org/10.1038/ncb2390

Zanetti, G., S. Prinz, S. Daum, A. Meister, R. Schekman, K. Bacia, and J.A. Briggs. 2013. The structure of the COPII transport-vesicle coat assembled on membranes. *eLife.* 2:e00951. https://doi.org/10.7554/eLife.00951

Zeuschner, D., W.J. Geerts, E. van Donselaar, B.M. Humbel, J.W. Slot, A.J. Koster, and J. Klumperman. 2006. Immuno-electron tomography of ER exit sites reveals the existence of free COPII-coated transport carriers. *Nat. Cell Biol.* 8:377–383. https://doi.org/10.1038/ncb1371

Shomron et al.
COPII defines the boundary between ER and ERESs

Journal of Cell Biology 16 of 16
https://doi.org/10.1083/jcb.201907224
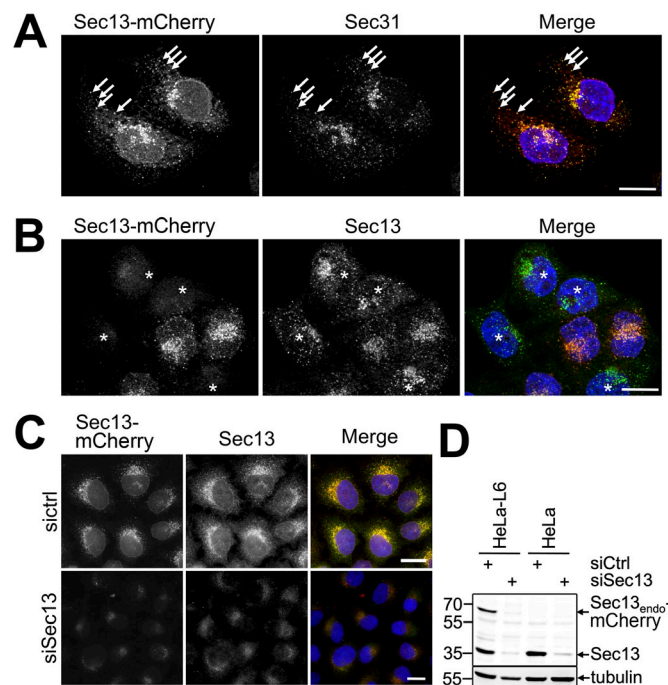
Figure S1. **Characterization of HeLa cells with Sec13 endogenously tagged with mCherry. (A)** Single apotome section of a pool of HeLa-L6 cells expressing endogenously tagged (endo) Sec13-mcherry costained with Sec31 antibodies. Sec13-mcherry nicely localizes to ERES. Scale bar = 5 µm. **(B)** Single apotome section of a pool of HeLa cells expressing Sec13-mcherry costained with Sec13. The untagged cells (asterisks) express similar levels of Sec13 as the Sec13-mcherry expressing cells, demonstrating that Sec13-mcherry is expressed at or below endogenous levels. Scale bar = 5 µm. **(C)** siRNA against Sec13, but not control (ctrl) siRNA, reduced expression of Sec13-mcherry as visualized by mCherry fluorescence and immunostaining against Sec13. Scale bars = 5 µm. **(D)** Western blot of HeLa and HeLa-L6 cells expressing Sec13-mcherry using Sec13 antibodies demonstrates efficiency of Sec13 siRNA. Sec13-mcherry is expressed below Sec13 levels and is efficiently reduced by Sec13 siRNA, validating that the identity of the Sec13-mcherry fusion.
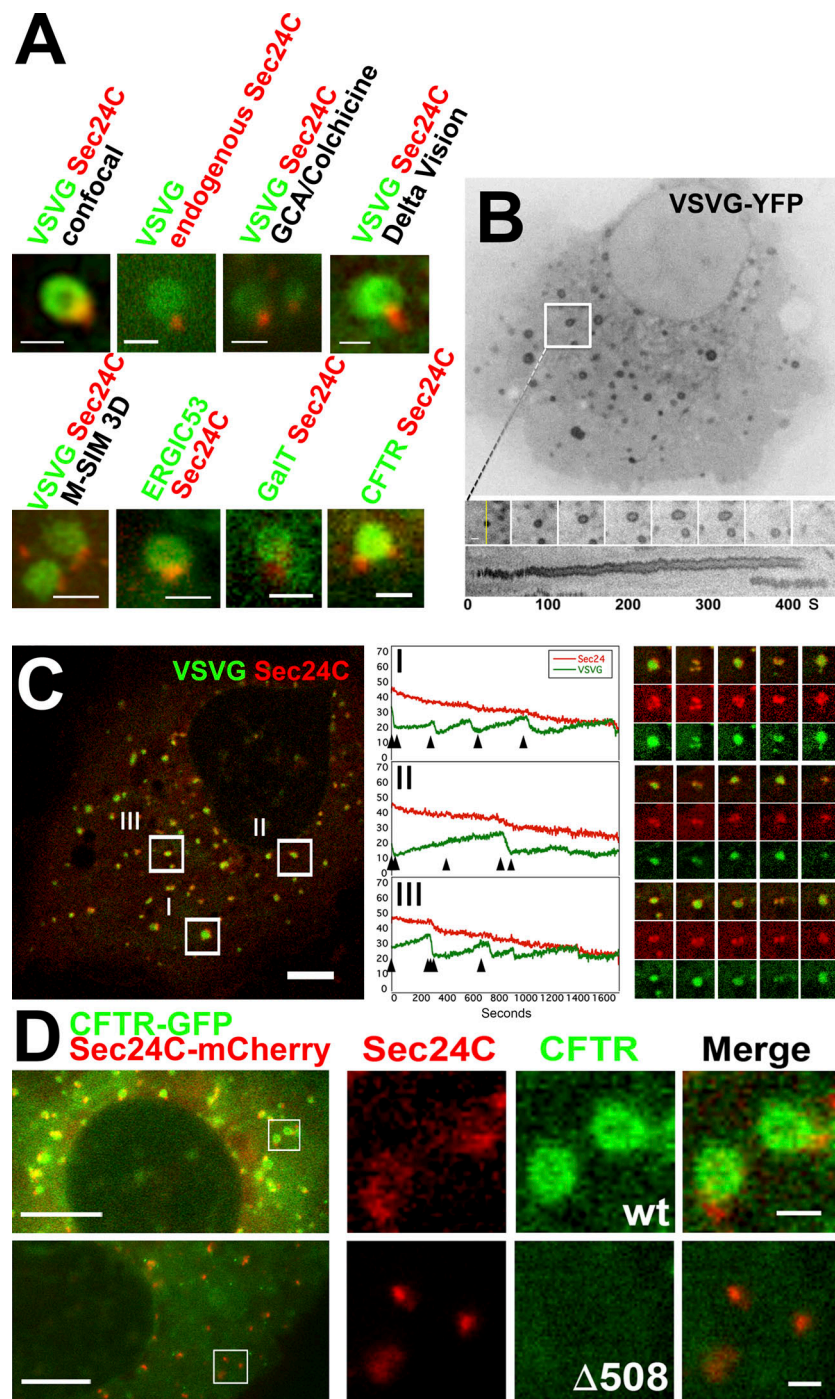
Figure S2. **Structure and function of ER exit sites in BFA/Noc treated cells. (A)** Relative localization of Sec24C-mCherry (red) and VSVG (green) within ERES of BFA/Noc-treated COS7 cells. Top, left to right: (1) Confocal microscope. (2) Immunofluorescence analysis of endogenous Sec24C (red) in a cell expressing VSVG-YFP (green). (3) Cells under Golgicide A/Colchicin treatment. (4) Deconvolution using DeltaVision microscope. Bottom, left to right: (1) Multifocal structured illumination microscopy (M-SIM). (2) Relative localization of Sec24C-mCherry (red) and ERGIC53-YFP, GalT-YFP, or CFTR-GFP (green) within a representative ERES of COS7 cells under BFA/Noc treatment. Scale bars = 1 µm. **(B)** Cargo and membrane accumulation in a single dilated exit site. A COS7 cell transfected with cargo protein VSVG-YFP and treated with BFA/Noc was monitored by a spinning disk confocal microscope captured at 5 frames/s. Representative time-lapse images of a single dilated exit site marked by the white square frame, are shown in the middle panel. Bottom: A kymogram generated from the line marked by the yellow line. Scale bar = 1 µm. **(C)** Analysis of COPII-mediated cargo sorting dynamics in ERESs of BFA/Noc-treated living COS7 cells. A cell coexpressing VSVG-YFP (green) and Sec24C-mCherry (red) was imaged using a spinning disk confocal microscope at 0.2-s intervals at the permissive temperature 32°C. The fluorescence intensity of VSVG-YFP (green line) and Sec24C-mCherry (red line) in three representative ERESs I through III (in white frames) are plotted, and representative images are shown on the right. Black arrowheads in the graph show time points of images on the right. Scale bar = 5 µm. **(D)** The mutant cargo protein CFTRΔ508-GFP (green, bottom) is excluded from ERES in BFA/Noc-treated COS7 cells. The cells are coexpressing Sec24C-mCherry (red) with either WT CFTR-GFP (green, top) or CFTRΔ508-GFP (green, bottom). Insets are enlarged fivefold. Left scale bars = 10 µm. Right scale bars = 1 µm.

Shomron et al.
COPII defines the boundary between ER and ERESs

Journal of Cell Biology   S2
https://doi.org/10.1083/jcb.201907224
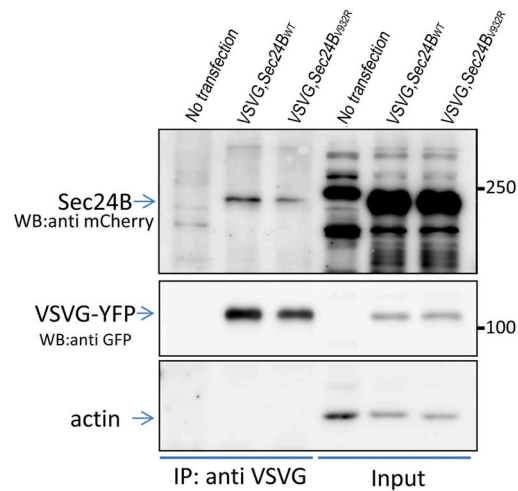
Figure S3. The Sec24B_{V932R} mutant interacts with VSVG. Immunoprecipitation (IP) analysis demonstrating interaction between the Sec24B_{V932R} mutant and VSVG. Cells coexpressing VSVG-YFP and WT or mutant Sec24B were immunoprecipitated with anti-VSVG antibodies, separated on SDS-PAGE, blotted, and probed with anti-GFP and anti-mCherry for VSVG and Sec24B, respectively. WB, Western blot.
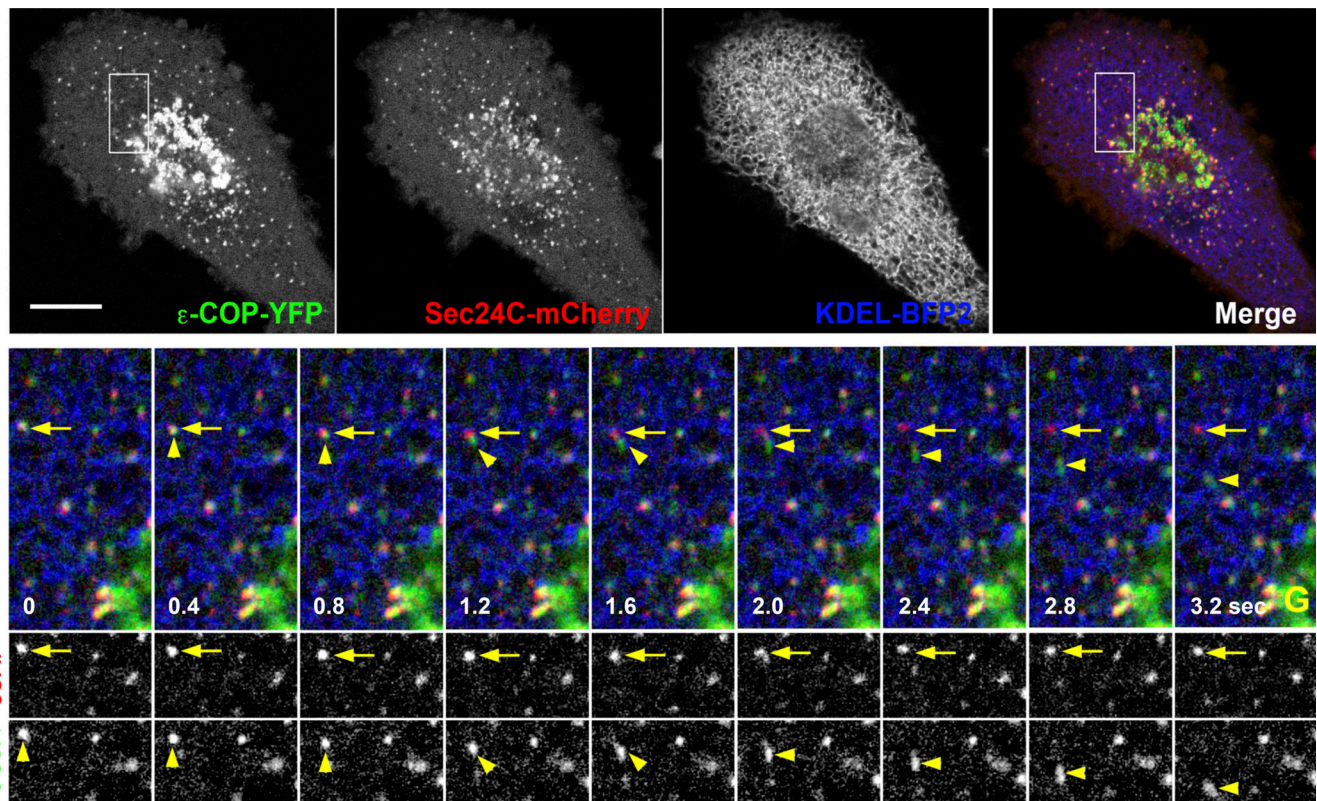
Figure S4. Colocalization to and translocation from ERESs of COPI-coated membranes. Time-lapse microscopy analysis of living LDLF cells stably expressing ε-COP-YFP (green) cotransfected with Sec24C-mCherry (red) and KDEL-BFP (Blue). Yellow arrows point to ERES labeled with Sec24C, and yellow arrowheads point to COPI membranes moving toward the Golgi (G). Scale bar = 10 μm.

Video 1. A HeLa cell clone expressing an endogenous Sec13-mCherry (red) inserted using the CRSPR/CAS12 knock-in method was transfected with VSVG-EGFP (green). Cells were transferred to permissive temperature (32°C) after overnight in 39.5°C, and images were taken at 15-s intervals for ~40 min (related to Fig. 1 B).

Video 2.   **Comparison between membrane-associated COPII movement and transport of ER-to-Golgi carriers.** COS7 cell coexpressing VSVG-YFP (green) and the COPII subunit Sec24C-mCherry (red) after shift to permissive temperature (32°C; related to Fig. 2 A).

Video 3.   **Comparison between membrane-associated COPII and microtubule plus-end polymerization using EB3-GFP.** A 3.7-s interval time-lapse sequence of COS7 coexpressing EB3-GFP (green) and the COPII subunit Sec24C-mCherry (red; related to Fig. 2 B).

Video 4.   **Accumulation of VSVG-YFP cargo and fission of carriers from ERESs in living cells.** Confocal images were captured after shift to permissive temperature of COS7 cells coexpressing COPII subunit Sec24C-mCherry (red) and the cargo protein VSVG-YFP (green; related to Fig. 3 A).

Video 5.   **Cargo accumulation in a single ERES and carrier fission.** Confocal images captured at 2.6-s intervals of COS7 cells transfected and treated as in A. VSVG-YFP (green) accumulation occurs downstream of Sec24C-mCherry (red; related to Fig. 3 B).

Video 6.   **Cargo accumulation in a single ERES and carrier fission.** Confocal images captured at 2.6-s intervals of COS7 cells transfected and treated as in Fig. 3 A. VSVG-YFP (green) accumulation occurs downstream of Sec24C-mCherry (red; related to Fig. 3 B).

Video 7.   **Cargo accumulation in a single ERES and carrier fission.** Confocal images captured at 2.6-s intervals of COS7 cells transfected and treated as in Fig. 3 A. VSVG-YFP (green) accumulation occurs downstream of Sec24C-mCherry (red; related to Fig. 3 B).

Video 8.   **Cargo accumulation in a single ERES and carrier fission.** Confocal images captured at 2.6-s intervals of COS7 cells transfected and treated as in Fig. 3 A. VSVG-YFP (green) accumulation occurs downstream of Sec24C-mCherry (red; related to Fig. 3 B).

Video 9.   **Photobleaching of the Golgi to expose ER-to-Golgi carrier life history.** The Golgi region of interest was photobleached in the VSVG-GFP (green) channel after transfer to permissive temperature (32°C) after overnight at 39.5°C. Cells used were HeLa cell clones expressing an endogenous Sec13-mCherry (red) transfected with VSVG-GFP (green; related to Fig. 4, A and B).

Video 10.   **Rab1b localizes with cargo throughout the life history of ER-to-Golgi carriers.** Huh7 cells cotransfected with VSVG-YFP (green and middle) and Rab1-mCherry (red and right) were shifted to permissive temperature of 32°C after overnight in nonpermissive temperature (39.5°C; related to Fig. 4 C).

Video 11.   **COPII-labeled membranes separate between ER and ERES membranes.** Confocal deconvolved images of a COS7 cell transfected and treated as described in Fig. 5 A (related to Fig. 5 C).

Video 12.   **COPII-labeled membranes separate between ER and ERES membranes.** Confocal deconvolved images of a COS7 cell transfected and treated as described in Fig. 5 A (related to Fig. 5 C).

Video 13.   **ERESs are connected to the ER in BFA/Noc-treated cells.** Confocal image of a living COS7 cell cotransfected with VSVG-YFP (green and right) and the soluble secreted luminal marker signal sequence-mCherry (red and middle) under BFA/Noc treatment (related to Fig. 5 D).

Video 14.   **Cargo and membrane accumulation in a single dilated exit site.** A COS7 cell transfected with cargo protein VSVG-YFP and treated with BFA/Noc was monitored by a spinning disk confocal microscope captured at 5 frames/s (related to Fig. S2 B).

Video 15.   **Analysis of COPII-mediated cargo sorting dynamics in ERESs of BFA/Noc-treated living COS7 cells.** ERESs in a cell coexpressing VSVG-YFP (green) and Sec24C-mCherry (red) was imaged using a spinning disk confocal microscope at 0.2-s intervals at the permissive temperature 32°C (related to Fig. S2 C).

Video 16.   **Golgi-associated ERESs disappear upon BFA-induced Golgi membranes blink-out.** Time-lapse sequence taken at 3-s intervals after addition of 5 µg/ml BFA to living cells coexpressing GalT-YFP and Sec24C-mCherry (related to Fig. 7 D).

Video 17.   **Translocation from ERESs of COPI-coated membranes.** Time-lapse microscopy analysis of living LDLF cells stably expressing ε-COP-YFP (green) cotransfected with Sec24C-mCherry (red) and KDEL-BFP (blue; related to Fig. S4).